HHS Public Access

Author manuscript

Cancer Res. Author manuscript; available in PMC 2024 August 01.

Published in final edited form as:

Cancer Res. 2024 February 01; 84(3): 388–404. doi:10.1158/0008-5472.CAN-23-1730.

PTEN Lipid Phosphatase Activity Suppresses Melanoma Formation by Opposing an AKT/mTOR/FRA1 Signaling Axis

Xiaonan Xu[1,#], **Ilah Bok**[1,2,#], **Neel Jasani**[1,2], **Kaizhen Wang**[1,2], **Manon Chadourne**[1], **Nicol Mecozzi**[1,2], **Ou Deng**[3], **Eric A. Welsh**[4], **Fumi Kinose**[5], **Uwe Rix**[3,6], **Florian A. Karreth**[1,6,†]

[1]Department of Molecular Oncology, H. Lee Moffitt Cancer Center and Research Institute, Tampa, Florida

[2]Cancer Biology PhD program, University of South Florida, Tampa, Florida

[3]Department of Drug Discovery, H. Lee Moffitt Cancer Center and Research Institute, Tampa, Florida

[4]Biostatistics and Bioinformatics Shared Resource, H. Lee Moffitt Cancer Center & Research Institute, Tampa, Florida

[5]Department of Thoracic Oncology, H. Lee Moffitt Cancer Center and Research Institute, Tampa, Florida

[6]Department of Oncologic Sciences, University of South Florida, Tampa, Florida

Abstract

Inactivating mutations in PTEN are prevalent in melanoma and are thought to support tumor development by hyperactivating the AKT/mTOR pathway. Conversely, activating mutations in AKT are relatively rare in melanoma, and therapies targeting AKT or mTOR have shown disappointing outcomes in preclinical models and clinical trials of melanoma. This has led to the speculation that PTEN suppresses melanoma by opposing AKT-independent pathways, potentially through non-canonical functions beyond its lipid phosphatase activity. In this study, we examined the mechanisms of PTEN-mediated suppression of melanoma formation through the restoration of various PTEN functions in PTEN-deficient cells or mouse models. PTEN lipid phosphatase activity predominantly inhibited melanoma cell proliferation, invasion, and tumor growth, with minimal contribution from its protein phosphatase and scaffold functions. A drug screen underscored the exquisite dependence of PTEN-deficient melanoma cells on the AKT/mTOR pathway. Furthermore, activation of AKT alone was sufficient to counteract several aspects of PTEN-mediated melanoma suppression, particularly invasion and the growth of allograft tumors. Phosphoproteomics analysis of the lipid phosphatase activity of PTEN

[†]Corresponding Author: Florian A. Karreth, florian.karreth@moffitt.org, office phone: +1-813-745-1851, mailing address: H. Lee Moffitt Cancer Center and Research Institute, Stabile Research Building Rm 23043, 12902 Magnolia Drive, Tampa, FL 33612, USA.
[#]Equal contribution

AUTHOR CONTRIBUTIONS

Conceptualization – XX, IB, FAK; Formal Analysis – XX, IB, OD, EAW, UR, FAK; Funding Acquisition – FAK; Investigation – XX, IB, NJ, KW, MC, NM, OD, FK, UR, FAK; Methodology – XX, IB, OD, EAW, FK, UR, FAK; Project administration – FAK; Supervision – UR, FAK; Visualization – XX, IB, OD, EAW, UR, FAK; Writing – original draft – XX, FAK; Writing – review & editing – XX, IB, NJ, KW, MC, OD, EAW, FK, UR, FAK.

Conflicts: The authors declare no financial conflicts of interest

validated its potent inhibition of AKT and many of its known targets, while also identifying the AP-1 transcription factor FRA1 as a downstream effector. The restoration of PTEN dampened FRA1 translation by inhibiting AKT/mTOR signaling, and FRA1 overexpression negated aspects of PTEN-mediated melanoma suppression akin to AKT. This study supports AKT as the key mediator of PTEN inactivation in melanoma and identifies an AKT/mTOR/FRA1 axis as a driver of melanomagenesis.

Keywords

Melanoma; PTEN; AKT; PI3K; mTOR; FRA1; mouse model

INTRODUCTION

Recurrent somatic mutation or copy number alteration of common driver genes promote the initiation and early stages of progression of cutaneous malignant melanoma. One of the earliest events in melanomagenesis is the hyperactivation of the MAPK pathway (1), which is most frequently caused by activating mutations in *BRAF* or *NRAS* or inactivating mutations in *NF1* (2). Melanoma progression requires the additional inactivation of tumor suppressor genes, and *CDKN2A* (encoding the cell cycle regulators p16INK4a and p14ARF) and *PTEN* are most commonly affected (1,2). *PTEN* encodes a phosphatase that dephosphorylates the lipid second messenger Phosphatidylinositol-3,4,5-triphosphate (PIP_3) to Phosphatidylinositol-4,5-bisphosphate (PIP_2), thereby opposing the function of PI3K, which phosphorylates PIP_2 at the 3 position. Anchored in the cell membrane, PIP_3 recruits pleckstrin homology (PH) domain-containing proteins, enabling their activation and downstream signaling. AKT and its downstream effector mTOR (as part of the mTORC1 complex) constitute the most widely studied pathway that is activated by PI3K via PIP_3. The importance of the PI3K/AKT/mTOR pathway in maintaining normal physiology is highlighted by its frequent alteration in disease, and activating mutations and copy number gains of *PIK3CA* (encoding the p110α catalytic subunit of PI3K) or *AKT* as well as inactivating mutations and copy number losses of *PTEN* are frequently observed in several cancers, including melanoma (3–7). Notably, alterations of *PTEN* are far more frequently observed in melanoma than alterations of *PIK3CA* or *AKT* (8), suggesting that PTEN inactivation more potently promotes melanomagenesis.

Given the frequent hyperactivation of the PI3K/AKT pathway, significant effort has been invested into gaining a better understanding of the role of this pathway in melanomagenesis and exploring its suitability as a therapeutic target. AKT is considered the key mediator of elevated PIP_3 levels, regulating numerous effectors to promote melanomagenesis. Indeed, melanoma mouse models overexpressing myristoylated AKT1 or the activated $AKT1^{E17K}$ mutant revealed a pro-metastatic effect of AKT (9,10). Interestingly, while independent AKT1 activation or PTEN deletion resulted in primary melanomas with similar latency and penetrance, activated AKT1 synergized with PTEN deficiency to promote metastasis in this mouse model (9). This suggests that the activation of AKT and possibly other downstream signaling pathways in response to the loss of PTEN changes during melanoma progression and metastasis. Several mouse melanoma models driven by $BRAF^{V600E}$ and melanocyte-

specific deletion of PTEN demonstrated that pharmacological inhibition of PI3K (11,12) or mTOR (13) as well as genetic restoration of PTEN (14) had superior antitumor effects than AKT inhibition (12). Moreover, PI3K maintains melanoma cell proliferation by regulating protein synthesis via mTORC1 independently of AKT (15). Elevated PIP_3 levels stimulate several kinases in addition to AKT (16), of which PDK1 and the SGKs have been reported as drivers of a malignant phenotype in PTEN-deficient melanoma (17,18). Thus, although AKT is widely considered a key signaling node in PTEN-deficient melanoma, it remains to be determined if AKT critically mediates the pro-tumorigenic effects of *PTEN* loss in melanoma.

PTEN possesses non-canonical functions that are independent of its lipid phosphatase activity. Indeed, PTEN was originally described as a protein phosphatase (19,20). Several protein phosphatase targets for PTEN have been identified, including FAK (21), SRC (22), IRS1 (23), PGK1 (24) RAB7 (25), and the glucocorticoid receptor (26). Interestingly, PTEN protein phosphatase activity has been associated with cancer cell migration (21,22,27–29), and a recent study suggested a role for the protein phosphatase activity of PTEN in melanoma metastasis (30). Even phosphatase-independent functions for PTEN as a scaffold have been discovered (31,32). These non-canonical functions raise the possibility that the loss or inactivation of PTEN promote melanoma, at least in part, through PIP_3- and AKT-independent mechanisms. These findings highlight the critical need for a better understanding of the mechanisms whereby PTEN suppresses melanoma, which promises to reveal new avenues for therapeutic intervention.

Here, we report that the lipid phosphatase activity confers PTEN with the ability to suppress melanoma, with negligible contribution of the protein phosphatase activity. The PTEN scaffold function is dispensable for melanoma suppression. Moreover, AKT is sufficient to overcome melanoma suppression mediated by restoring PTEN expression, affirming AKT as the predominant downstream effector of PTEN loss-of-function. AKT controls the expression of the AP1 transcription factor FRA1 via mTOR-mediated translation, and FRA1 partially negates the effects of PTEN restoration. Thus, our results nominate an AKT/mTOR/FRA1 axis as a key driver of melanoma.

MATERIALS AND METHODS

Cell lines and culture condition

Mouse melanoma cell lines M10M1 and M10M6 were isolated from melanomas from $Braf^{V600E}$; $Pten^{null}$ (BPP) mice as described previously (14). Human melanoma cell lines WM115 (RRID:CVCL_0040), WM266–4 (RRID:CVCL_2765), and 1205Lu (RRID:CVCL_5239) were obtained from Meenhard Herlyn (Wistar Institute) and SBCL2 (RRID:CVCL_D732) were obtained from David Tuveson (Cold Spring Harbor Laboratory). HEK293T Lenti-X were obtained from Takara. All cell lines were cultured in a humidified atmosphere at 37°C and 5% CO2. Melanoma cell lines were cultured in RPMI 1640 (Lonza) containing 5% FBS (Sigma). HEK293T Lenti-X were cultured in DMEM (VWR) containing 10% FBS. All cell lines were confirmed bimonthly to be Mycoplasma-free with the MycoAlert Mycoplasma Detection Kit (Lonza) and STR authenticated when they were initially obtained. Cell lines were used for experiments within 15 passages after thawing.

Animal models

All animal experiments were conducted in accordance with an Institutional Animal Care and Use Committee protocol approved by the University of South Florida. The development of $Braf^{V600E}$; $Pten^{null}$ (BPP) ESC-GEMM was described previously (14). BPP ES cells were targeted with TRE-$Pten^{WT}$ or mutant constructs (TRE-$Pten^{C124S}$, TRE-$Pten^{G129E}$, TRE-$Pten^{Y138L}$) designed to co-express GFP via an IRES. To induce melanomagenesis, mice were anesthetized with Isoflurane and their back hair was shaved with clippers. 4OHT (Sigma Aldrich) dissolved in DMSO (2.5 mg/mL) was administered with a paintbrush on the back skin of 3–4 week old mice on two consecutive days. Nude mice ($Foxn1^{Nu/Nu}$) were obtained from JAX (Stock #007850). NSG mice were obtained from JAX (Stock #005557) and bred in-house. 2.5×10^5 M10M6 melanoma cells were subcutaneously injected into the flank of nude mice or NSG mice. Tumors were measured using calipers and volume was calculated using the formula ($width^2 \times length$)/2. Mice were fed chow containing 200 mg/kg Doxycycline (Envigo).

TCGA data and GEO dataset

The GEO dataset GSE112509 containing RNA expression data from 23 nevi and 57 melanomas was used to analyze differential expression of potential targets of PTEN lipid phosphatase in nevi and melanomas using T-test. A P value <0.05 and a fold-change of Mean > 2 were used as the threshold. Gene expression data and patient follow-up data from 457 skin cutaneous melanoma (SKCM) cases in The Cancer Genome Atlas (TCGA) were analyzed for the correlation between FOSL1 expression and patient survival using Kaplan–Meier analysis.

Plasmid and lentivirus production

pLenti-TRE-GFP-Blast was generated by replacing the CMV promoter in pLenti-GFP-Blast with the TRE3G promoter from pRRL-TRE3G-GFP-PGK-Puro-IRES-rtTA3 (from J. Zuber). pLenti-TRE-$Pten^{WT}$-Blast and pLenti-TRE-$Pten^{C124S}$-Blast were created by replacing GFP in pLenti-TRE-GFP-Blast with mouse Pten wildtype or mutant cDNA. pLenti-TRE-$Pten^{G129E}$-Blast and pLenti-TRE-$Pten^{Y138L}$-Blast were generated by site-directed mutagenesis using pLenti-TRE-$Pten^{WT}$-Blast as a template. Q5 Site-Directed Mutagenesis Kit (New England BioLabs) was used following the manufacturer's instruction. pLenti-CMV-Akt^{E17K}-Hygro was generated by replacing GFP in pLenti-CMV-GFP-Hygro with AKT^{E17K} cDNA from pFBD-Akt1(E17K) (Addgene plasmid #86563). pLenti-CMV-Fosl1-Hygro was generated by replacing GFP in pLenti-CMV-GFP-Hygro with Fosl1 cDNA from mouse embryonic fibroblasts (MEF). FRA1-translation-reporter (FRA1-TR) was generated by inserting 300bp of the sequence immediately upstream of the translation start site of FRA1 (251bp of the 5'UTR and 49bp of exon 1) into pLenti-CMV-GFP-Puro vector upstream of the GFP cDNA. To produce lentivirus supernatants, HEK293T cells were transfected with lentiviral vector and Δ8.2 and VSVG helper plasmids at a 9:8:1 ratio. Lentiviral supernatant was cleared using 0.45 μm syringe filters and used to infect melanoma cells in the presence of 8 μg/mL polybrene. Infected cells were selected with the appropriate antibiotics (1 μg/mL puromycin, 100 μg/mL hygromycin, or 10 μg/mL blasticidin).

Proliferation assays

1×10^3 M10M1 or M10M6 cells/well were seeded in 96 well plates in 200μL RPMI 1640 medium containing 5% FBS. After 24 hours, the plate was loaded into Cellcyte-X live cell analyzer (ECHO). Images of each well were taken daily for 4–5 days and the cell confluency of each image was quantified.

Low density growth assays

0.5×10^3 M10M1 or M10M6 cells were seeded in 6-well plates in triplicates and incubated for 8 days. Cells were fixed in cold 4% paraformaldehyde (VWR) and stained with 0.5% crystal violet (VWR). Percent area of crystal violet staining was quantified using Image J.

Soft agar assays

SeaPlaque Agarose (1.6% w/v) in PBS was mixed 1:1 with RPMI 1640 and 1mL of the 0.8% agarose was used to pour a bottom layer in 6-well plates. Melanoma cells were trypsinized, counted, and 5×10^3 cells were resuspended in 1 mL of RPMI 1640 medium containing 20% FBS. Cells were then mixed with 1 mL of 0.8% SeaPlaque Agarose in PBS and plated atop the solidified agar (0.4% final concentration). The top layer was allowed to solidify at room temperature, followed by culture at 37°C with 100 μL of fresh medium added every 3 days. Pictures were taken after 10 to 15 days and analyzed with ImageJ.

Transwell invasion assays

To pre-coat transwells, Matrigel (Corning) was thawed on ice for at least 2 hours, diluted to 5% with ice-cold RPMI 1640 medium, and gently added to transwell inserts (50 μL/insert) and solidified at 37°C for 30 min. Melanoma cells were trypsinized and resuspend in RPMI 1640 medium. For transwell invasion assays, 2×10^4 M10M1 or M10M6 cells were plated per Matrigel-coated insert in 200 μl of RPMI 1640 without FBS. 500 μl RPMI 1640 medium containing 15% FBS were added into the bottom well. Plates were incubated at 37°C in a humidified incubator for 48 hr. Media was discarded, inserts were gently washed once with PBS, and cells were fixed with 500 μl fixing solution (ethanol:acetic acid = 3:1) in the bottom well for 10 minutes. Inserts were washed once with PBS, and cells were stained in 500 μL staining solution (0.5% crystal violet) for 30 minutes. Inserts were washed with tap water twice and non-migrated cells or Matrigel on the top side of the insert were carefully removed with cotton swabs, and inserts were air dried overnight. Pictures were taken at 200x magnification and cell numbers quantified.

Small molecule inhibitor library screening

250 M10M6-Pten^{C124S} cells and 750 M10M6-Pten^{WT} cells were seeded in 384 well plate with 40 μL RPMI 1640 medium containing 5% FBS using Bravo automated liquid handling platform (Agilent). After 24 hours, the drug library was added to 40 μL cells with final concentrations of 0.1 μM, 0.5 μM, 2.5 μM, and 10 μM drug using Echo650 (Labcyte/ Beckman Coulter). The same volume of DMSO was used as negative control. After 5 days, 10 μL CellTiter Glo (Promega) were added to 40μL cells and gently shaken at room temperature for 10 minutes, luminescence was recorded using a PerkinElmer EnVision plate

reader. Cell viability = [luminescence (drug) / luminescence (DMSO)] × 100%. Sensitivity = [100% - (cell viability)] / 100%.

Phosphoproteomics

Cells were harvested, lysed with urea lysis buffer, sonicated using a microtip sonicator, and digested using the PTMScan Kit Protocol (Cell Signaling). Peptide purification was performed using Sep-Pak® C18 columns (Waters). Eluates were collected in the same tube and then aliquoted for pY enrichment (1 mg per sample) or global phosphoproteomics (200 μg per sample). Samples were frozen at −80°C overnight and lyophilized for two days to ensure that there was no TFA left in the samples. Phosphotyrosine-containing peptides were immunoprecipitated using PTMScan p-Tyr-1000 immunoaffinity beads (Cell Signaling #8803). Subsequently, samples were labeled using TMT reagents according to the manufacturer instructions (TMTpro™ 16plex Label Reagent Set, # A44521). Labeling efficiency was confirmed by MS. After sample combination and lyophilization, peptides were redissolved in 250 μl of 20 mM ammonium formate buffer (pH 10.0). Basic pH reversed-phase liquid chromatography separation was performed on an XBridge column (Waters). Fifteen concatenated peptide fractions were dried by vacuum. TMT channel 16 was used for boosting of pY signals with a 10 mg bulk GFP sample and channel 14 was left empty (33). Peptides for global phosphoproteomics (pSTY) were labeled using TMT 16-plex reagents as described above. Phosphopeptide enrichment was achieved using an IMAC enrichment kit (Sigma I1408). Samples were evaporated using a speed vacuum centrifuge and resuspended in 2% ACN / 0.1% FA, which contained 50 fmol/μl of PRTC (Thermo Scientific Pierce Retention Time Calibration Mixture, PIERCE) to confirm consistent performance of the LC-MS analyses. The acquired pY and IMAC data were searched with MaxQuant with the murine UniProt database using the embedded search engine, Andromeda. Carbamidomethylated cysteines were set as fixed modification and oxidation of methionine, N-terminal protein acetylation, and phosphorylation of serine, threonine, and tyrosine as variable modifications. Further, the MaxQuant initial search precursor and fragment ion tolerance were set to 20 ppm and m/z 0.05, respectively. The MaxQuant main search precursor ion mass tolerance was 4.5 ppm. Resolution was set to 70,000 at 200 m/z for MS1 and 17,500 for MS2. MaxQuant automatically filters out any TMT-labeled peptides that are isolated with less than 75% purity. The data were then filtered for 1% protein FDR, plus common contaminants. For the analysis and comparison of TMT 16-plex global pSTY data and pY data, the reporter ion intensity was used for the relative quantification of each peptide. IRON (iterative rank-order normalization) of MaxQuant data was performed as described before (34). The experiment was performed with three biological replicates. Each treated sample was run as two technical replicates. Biological triplicates were then averaged, and the log2 ratio was determined between the samples. The phosphorylated peptides were filtered for further analysis with absolute value of log2 fold change (> 0.585) and p value (<0.05). KEGG pathway enrichment analysis of differentially phosphorylated proteins from phosphoproteomics data sets was performed with Enrichr (https://maayanlab.cloud/Enrichr/) (35–37). Volcano Plots were created by GraphPad Prism 9.

qRT-PCR

RNA was extracted from cells using TRIzol (Invitrogen) following protocols supplied by the manufacturer. cDNA was generated with PrimeScript RT Master Mix (Takara). qPCR was performed on StepOnePlus Real-Time PCR System (Thermo Fisher Scientific) using PerfeCTa SYBR Green Fastmix (Quantabio). mRNA expression was normalized to 18S rRNA. Primer sequences were obtained from PrimerBank (https://pga.mgh.harvard.edu/primerbank/index.html; RRID:SCR_006898): Mouse Fosl1 forward: ATGTACCGAGACTACGGGGAA. Mouse Fosl1 reverse: CTGCTGCTGTCGATGCTTG. Human FOSL1 forward: CAGGCGGAGACTGACAAACTG. Human FOSL1 reverse: TCCTTCCGGGATTTTGCAGAT. RNA18S forward: CTAAATACCGGCACGAGACC. RNA18S reverse: TTCACGCCCTCTTGAACTCT.

Nuclear/Cytoplasmic Co-Immunoprecipitation

Nuclear and cytoplasmic fractions of A375 cells were lysed and isolated using NE-PER Nuclear and Cytoplasmic Extraction Kit (Thermo Fisher Scientific). Nuclear and cytoplasmic lysates were incubated with PTEN antibody (1:100) at 4°C overnight. 20 μL Pierce™ Protein A/G Magnetic Beads (Thermo Fisher Scientific) were washed with TBST (Tris-buffered saline containing 0.05% Tween-20) and incubated with lysate-antibody solution at 4°C for 1 hour. Supernatants were discarded and the beads were washed 3 times with TBST. Protein bound to the beads were eluted with SDS-PAGE sample buffer and subjected to Western Blot analysis.

Western blot analysis

15μg of total protein were separated on NuPAGE 4–12% precast gels (Thermo Fisher Scientific) and transferred to nitrocellulose membranes. Membranes were blocked in 5% non-fat dry milk in TBST and incubated with FRA1 (Abcam, ab252421) (1:1,000), or one of the following primary antibodies from Cell Signaling Technology (CST) at 1:1000 overnight at 4°C: PTEN (CST, #9188), phospho-AKT (Ser 473) (CST, #4060), AKT (pan) (CST, #4691), phospho-p70 S6 kinase (Thr389) (CST, #9234), p70 S6 kinase (CST, #2708), phospho-S6 ribosomal protein (Ser235/236) (CST, #5364), S6 ribosomal protein (CST, #2217), phospho-FAK (Try397) (CST, #8556), FAK (CST, #3285), phospho-PRAS40 (Thr246) (CST, #13175), PRASS40 (CST, #2691), ERK1/2 (CST, #4695), phospho-ERK1/2 (Thr202/Tyr204) (CST, #9101), 4E-BP1 (CST, #9452), phospho-4E-BP1 (Ser65) (CST, #9451), phospho-FRA1 (Ser 265) (CST, #5841). β-Actin (Invitrogen, AM4302) (1:3,000) was blotted as a loading control. Membranes were washed 3 times with TBST for 10 min, followed by incubation with HRP-conjugated secondary antibodies (1:3,000) for 1 hr at room temperature. After three washes in TBST, chemiluminescence substrate (1:1) was applied to the blots for 4 min and chemiluminescence signal was captured using a LI-COR imaging system.

Immunohistochemistry

Tumor tissues were harvested and fixed overnight in 10% neutral buffered formalin. Tissues were dehydrated in 70% ethanol the following day. IDEXX BioAnalytics (Columbia, MO) performed paraffin embedding, sectioning, and hematoxylin and eosin staining.

Antibodies against PTEN (1:100, Cell Signaling Technology, Cat. #9559) were used for immunohistochemistry.

Quantification and statistical analysis

Proliferation assays, low density growth assays, and soft agar assays are presented as mean ± SEM. For transwell invasion assays, three or four random fields were quantified for each well and data are presented as mean ± SEM. All experiments were performed at least three times with three to four technical replicates. Statistical analyses were performed by Student's unpaired t test. Data of subcutaneous tumor growth curve and tumor weight at endpoint are presented as mean ± SEM. Graphpad Prism 9 (RRID:SCR_002798) was used for statistical analyses and a P value of <0.05 was considered statistically significant.

Data availability

The RNA-seq data analyzed in this study were obtained from GEO at GSE112509 and TCGA (Skin Cutaneous Melanoma TCGA-SKCM) at https://portal.gdc.cancer.gov/. Patient survival data were obtained from TCGA-SKCM and analyzed using Gene Expression Profiling Interactive Analysis (GEPIA) (38). The data generated in this study are available within the article and its supplementary data files. The raw data of the small molecule inhibitor screen are available in Supplementary Table 1, and the raw data of the phosphoproteomics are available in Supplementary Table 2. All other raw data generated in this study are available upon request from the corresponding author.

RESULTS

The lipid phosphatase activity mediates the melanoma suppressor function of PTEN in vitro.

Using an ESC-GEMM platform, we showed previously that restoring endogenous Pten expression in melanomas and melanoma-derived cell lines significantly diminished tumor growth and cell proliferation, respectively (14). Similarly, in murine $Braf^{V600E}$; $Pten^{\Delta/\Delta}$ (BPP) melanoma cell lines harboring the rtTA3 reverse transactivator to enable Dox-mediated transcriptional control of expression cassettes, we demonstrated that expression of ectopic Pten reduces proliferation in vitro and allograft tumor growth (14,39). This represents an ideal system to assess the melanoma suppressive potential of the different PTEN functions. We therefore generated Dox-inducible expression constructs harboring either wildtype *Pten* ($Pten^{WT}$), one of three mutant *Pten* isoforms ($Pten^{C124S}$, $Pten^{G129E}$, or $Pten^{Y138L}$), or a *GFP* control cDNA. $Pten^{C124S}$ has no phosphatase activity, $Pten^{G129E}$ is lipid phosphatase-deficient but retains protein phosphatase activity, and $Pten^{Y138L}$ is protein phosphatase-deficient but retains lipid phosphatase activity. All Pten isoforms retain scaffolding activity.

To examine the contribution of PTEN functions to melanoma suppression, these constructs were expressed in BPP mouse melanoma cell lines M10M1 and M10M6 (Fig. 1A, Supplementary Fig. S1A). Similar to our previous findings (14), the restoration of $Pten^{WT}$ expression significantly attenuated proliferation of both cell lines (Fig. 1B). Protein phosphatase-deficient $Pten^{Y138L}$ moderately reduced proliferation of M10M1 cells, while

it phenocopied the robust suppression of proliferation in M10M6 cells (Fig. 1B). Neither phosphatase-dead Pten^{C124S} nor lipid phosphatase-deficient Pten^{G129E} affected melanoma cell proliferation (Fig. 1B). Pten^{WT} robustly reduced low-density colony formation of M10M1 and M10M6 cells, which was partially recapitulated by Pten^{Y138L}, while Pten^{C124S} and Pten^{G129E} had no effect (Fig. 1C). Moreover, the colony size and number under anchorage-independent growth conditions in soft agar were markedly reduced in M10M1 and M10M6 cells expressing Pten^{WT} or Pten^{Y138L} (Fig. 1D). Interestingly, Pten^{G129E} moderately reduced colony size and number in both cell lines, while Pten^{C124S} had no effect (Fig. 1D). Taken together, the PTEN lipid phosphatase function accounts for most of the suppressive activity in several cell proliferation assays, while the PTEN protein phosphatase function only contributes to suppression of anchorage-independent growth and putative PTEN scaffold functions play no role.

Interestingly, we observed cell morphological changes in M10M1 and M10M6 cells expressing the different PTEN mutants under low serum (M10M6) or normal (M10M1) growth conditions. Pten^{WT}- and Pten^{Y138L}-expressing cells appeared more epithelial, were smaller and exhibited contact inhibition, while cells expressing Pten^{G129E} and Pten^{C124S} were more elongated and spindle-like (Supplementary Fig. S1B). This suggested that PTEN restoration may also affect the invasive capability of melanoma cells. Indeed, expression of Pten^{WT} markedly inhibited melanoma cell invasion in transwell assays, and this was completely phenocopied by Pten^{Y138L} (Fig. 1E). Pten^{G129E} and Pten^{C124S} exhibited no effect on invasion of M10M1 and M10M6 cells (Fig. 1E). Thus, PTEN suppresses melanoma cell invasion entirely through its lipid phosphatase function.

The lipid phosphatase function of PTEN suppresses melanoma initiation and growth in vivo.

We next determined which function of PTEN suppresses melanoma in vivo by performing allografts in immunocompromised NSG and Nu/Nu mice. We subcutaneously injected M10M6 cells harboring the Doxycycline (Dox)-inducible *Pten* expression constructs or *GFP* control, placed the mice on a Dox diet immediately following the transplantation, and monitored tumor growth. Tumors expressing Pten^{G129E} or Pten^{C124S} grew at a similar rate compared to GFP control tumors, and expression of Pten^{WT} or Pten^{Y138L} markedly inhibited tumor growth (Fig. 2A, Supplementary Fig. 2A). Immunohistochemistry analysis of tumors from NSG mice revealed markedly reduced Pten expression in Pten^{WT} and Pten^{Y138L} tumors compared to Pten^{C124S} and Pten^{G129E} tumors (Fig. 2B). Similarly, Pten^{WT} or Pten^{Y138L} tumors grown in Nu/Nu mice had lost expression of Pten, while Pten^{C124S} and Pten^{G129E} tumors maintained Pten expression (Supplementary Fig. 2B). These findings suggests that there is strong selective pressure against PTEN lipid phosphatase activity during melanoma growth. Accordingly, the levels of Akt phosphorylated at Ser473 were comparable between tumors expressing lipid phosphatase active (Pten^{WT} or Pten^{Y138L}) and inactive (Pten^{C124S} and Pten^{G129E}) PTEN (Supplementary Fig. 2B). To exclude the possibility that selection against Pten expression occurred in vitro prior to transplantation, we let tumors grow in the absence of Dox, then administered Dox for 2 days prior to endpoint, and analyzed Pten expression. Pten^{WT}, Pten^{Y138L}, Pten^{G129E}, and Pten^{C124S} tumors expressed similar Pten levels (Supplementary Fig. 2C), validating that the Tet-On

system remained functional and that tumor growth requires a reduction in the PTEN lipid phosphatase activity.

To further determine the role of the PTEN lipid and protein phosphatase activities in the initiation and early stages of spontaneous melanomagenesis, we used our ESC-GEMM platform. We targeted BPP (LSL-Braf^{V600E}; Pten$^{FL/FL}$; Tyr-CreERt2; CAGs-LSL-rtTA3; CHC) ES cells (14) with Dox-inducible *Pten* expression constructs (TRE-Pten^{WT}-IRES-GFP, TRE-Pten^{C124S}-IRES-GFP, TRE-Pten^{G129E}-IRES-GFP, and TRE-Pten^{Y138L}-IRES-GFP) (Fig. 2C). Because we suspected that there could be negative selection against ectopic *Pten* expression in tumors, we linked a *GFP* cDNA to the *Pten* cDNAs via an internal ribosome entry site (IRES). This enabled the use of GFP as an indicator of ectopic Pten expression and circumvented the difficulties with distinguishing between endogenous wildtype and ectopic mutant Pten expression. Targeted BPP ES cells were used to generate experimental chimeras and melanomagenesis was induced by topical administration of 4-Hydroxytamoxifen (4OHT) on shaved backs at 3 weeks of age. 4OHT activates the melanocyte-specific Cre, which in turn induces Braf^{V600E} expression, deletes both Pten alleles, and activates expression of the rtTA3 reverse transactivator. The mice were placed on a Dox-containing diet immediately following 4OHT administration to activate expression of the transgenic Pten cDNA constructs (Fig. 2C). Melanomas formed readily in each of the four Pten cohorts, leading to indistinguishable tumor-free survival and overall survival as well as tumor numbers (Supplementary Fig. S2D–E). To test if expression of the ectopic Pten alleles was induced, we collected tumor tissue and determined GFP expression as a surrogate for transgenic activation by Western blot. Notably, the frequency of GFP-positive tumors in the Pten^{C124S} and Pten^{G129E} cohorts was significantly higher than in the Pten^{WT} and Pten^{Y138L} cohorts (66% in Pten^{C124S} and 64% in Pten^{G129E} vs. 29% in Pten^{WT} and 11% in Pten^{Y138L}) (Fig. 2D), again suggesting that there is strong selective pressure against the expression of PTEN lipid phosphatase activity. These in vivo findings corroborated the in vitro data indicating that PTEN suppresses melanoma primarily through its lipid phosphatase function.

A small molecule inhibitor screen highlights the importance of the AKT/mTOR axis in PTEN-deficient melanoma.

After establishing that PTEN suppresses melanoma through its lipid phosphatase activity, we sought to determine key effectors that mediate the suppressive effects of PTEN. To this end, we performed a small molecule inhibitor screen in M10M6 cells in which Pten is inactive (Pten^{C124S}) or in which Pten activity is restored (Pten^{WT}). We reasoned that Pten restoration would inactivate critical pathways, thereby reducing the sensitivity to drugs targeting those pathways. Thus, the differential drug sensitivity between Pten^{C124S} and Pten^{WT} melanoma cells may identify critical effectors. We used an expanded drug panel that is based on an earlier library (40), which contains 500 small molecule inhibitors (of which approximately 20% are FDA-approved, 40% are currently in clinical trials, 20% were previously in clinical trials, and 20% are preclinical compounds/chemical probes for unique targets) at four concentrations (0.1 μM, 0.5 μM, 2.5 μM, and 10 μM). We induced Pten^{C124S} and Pten^{WT} expression by incubating M10M6 cells with Dox for 24 hours, followed by treating cells with the drug library for 5 days. Drug sensitivity was measured

via cell viability and compared to DMSO treated cells. At the 2.5 μM concentration, 287 out of 500 inhibitors were more effective in $Pten^{C124S}$ cells compared to $Pten^{WT}$ cells (Supplementary Table S1), possibly reflecting the widespread signaling changes that occur upon Pten inactivation. Notably, $Pten^{C124S}$ cells were more sensitive to all AKT inhibitors (7/7), all mTORC1 inhibitors (4/4), and most mTOR inhibitors (8/10) compared to $Pten^{WT}$ cells, suggesting robust addiction of Pten-deficient cells to the Akt/mTor pathway (Fig. 3A, Supplementary Table S1). To examine this further, we treated $Pten^{WT}$, $Pten^{C124S}$, $Pten^{G129E}$, or $Pten^{Y138L}$ expressing M10M6 cells with a high dose of the AKT inhibitor MK2206 (2.5 μM). MK2206 inhibited cell proliferation more robustly in $Pten^{C124S}$ and $Pten^{G129E}$ expressing cells compared to $Pten^{WT}$ and $Pten^{Y138L}$ expressing cells consistent with the effects observed in the drug screen (20.1% vs. 22% inhibition for $Pten^{WT}$ and 33.3% vs. 32% inhibition for $Pten^{C124S}$) (Supplementary Fig. S3A). Moreover, we found that $Pten^{C124S}$ and $Pten^{G129E}$ expressing cells are markedly more sensitive to MK2206 compared to $Pten^{WT}$ and $Pten^{Y138L}$ in colony formation and transwell invasion assay (Supplementary Fig. S3B–C). This confirms that PTEN lipid phosphatase function reduces AKT signaling, rendering PTEN restored cells less sensitive to AKT inhibition.

Reactivating AKT partially rescues PTEN induced melanoma suppression.

We next determined whether inhibiting the AKT/mTOR pathway is sufficient to mediate the tumor suppressive effects of PTEN. To this end, we expressed constitutively active Akt (Akt^{E17K}) in $Pten^{WT}$ M10M1 and M10M6 cells (Supplementary Fig. S3D) and examined whether this negates the tumor suppressive effects of Pten. Reactivation of Akt partially rescued the suppression of cell proliferation induced by $Pten^{WT}$ in both melanoma cell lines (Fig. 3B). Moreover, Akt reactivation was less potent in low density and anchorage-independent growth assays where it only moderately rescued the effects of $Pten^{WT}$ restoration (Fig. 3C,D). Conversely, reactivating Akt fully rescued the $Pten^{WT}$-mediated suppression of cell invasion in transwell assays (Fig. 3E). To determine whether active Akt can overcome $Pten^{WT}$-mediated melanoma suppression, we performed subcutaneous allografts in NSG mice. Notably, active Akt completely rescued the repression of melanoma growth by $Pten^{WT}$ (Fig. 3F,G, Supplementary Fig. S3E). These results, combined with the data obtained with the PTEN phosphatase mutants, suggest that PTEN suppresses melanoma invasion in vitro and tumor growth by inhibiting AKT, while melanoma cell proliferation under different in vitro conditions is suppressed through additional pathways.

A previous study reported minimal effects of the AKT inhibitor MK2206 on melanoma cell proliferation (15), while our results indicate that PTEN suppresses proliferation through its lipid phosphatase activity at least in part by inactivating AKT. We therefore evaluated this further by examining the effect of MK2206 in our murine melanoma cell lines. Even at low doses of MK2206 (0.1–0.5 μM), Akt activation as measured by Ser473 phosphorylation was reduced to an extent similar to that elicited by $Pten^{WT}$ restoration (Fig. 4A). In agreement with the study by Silva et al. (15), even the highest dose (1 μM) of MK2206 failed to inhibit melanoma cell proliferation and low density growth, while $Pten^{WT}$ restoration elicited marked suppression (Fig. 4B,C, Supplementary Fig. S4A). By contrast, MK2206 inhibited melanoma cell invasivon in a dose dependent manner, with the highest dose eliciting effects comparable to $Pten^{WT}$ restoration (Fig. 4D, Supplementary Fig. S4B). Taken together, these

findings further support the notion that the PTEN lipid phosphatase activity suppresses some aspects of melanomagenesis predominantly by inactivating AKT signaling.

Phosphoproteomics analysis reveals potential PTEN lipid phosphatase targets

To comprehensively identify the pathways downstream of PTEN lipid phosphatase activity, we performed phosphoproteomics in M10M6 melanoma cells expressing GFP, $Pten^{WT}$, $Pten^{C124S}$, $Pten^{G129E}$, or $Pten^{Y138L}$. We induced Pten expression for 16 hours with Dox (Supplementary Fig. S5A) and then denatured, reduced, alkylated, and digested the isolated proteins. Using LC-MS/MS, we performed 16-plexed global phosphoproteomics to detect phosphorylation changes at Serine, Threonine, and Tyrosine residues (pS/T/Y) and an additional 16-plexed phospho-Tyrosine proteomics analysis to enrich for phosphorylation changes at Tyrosine residues (pY) (Fig. 5A). Principle component analysis (PCA) showed that the phosphorylation patterns in the GFP control and $Pten^{C124S}$ cells were highly similar, as expected given the lack of a suppressive effect of the PTEN scaffold function. Phosphorylation in $Pten^{G129E}$ cells was also similar to GFP/$Pten^{C124S}$ cells, suggesting that the PTEN protein phosphatase function does not provoke pronounced phosphorylation changes of the proteome. By contrast, phosphorylation changes in $Pten^{WT}$ and $Pten^{Y138L}$ cells were remarkably similar to each other but distinct from GFP/$Pten^{C124S}$/$Pten^{G129E}$ cells (Fig. 5B). Given the high similarity between GFP and $Pten^{C124S}$ cells, we combined them to a single negative control and compared it to $Pten^{WT}$, $Pten^{G129E}$, and $Pten^{Y138L}$ cells to identify proteins differentially phosphorylated in response to PTEN lipid phosphatase activity. We found that phosphorylation of 594 proteins (a total of 1160 sites) were decreased while 119 proteins (240 sites) were increased by $Pten^{WT}$ (Fig. 5C, Supplementary Table S2), and $Pten^{Y138L}$ led to decreased phosphorylation of 264 proteins (451 sites) and increased phosphorylation of 80 proteins (161 sites) (Fig. 5D, Supplementary Table S2). Phosphorylation of 105 proteins (138 sites) was decreased while phosphorylation of 30 proteins (40 sites) was increased by $Pten^{G129E}$ (Fig. 5E, Supplementary Table S2). Notably, the extent of phosphorylation changes and the affected proteins largely overlap in $Pten^{WT}$ and $Pten^{Y138L}$ cells (Fig. 5C,D, Supplementary Fig. S5B, Supplementary Table S2). Kyoto Encyclopedia of Genes and Genomes (KEGG) analysis revealed that ErbB signaling, insulin signaling, and autophagy pathways – pathways that have been associated with AKT signaling – are enriched in $Pten^{WT}$ and $Pten^{Y138L}$ cells (Fig. 5F,G). Conversely, the pathways enriched in $Pten^{G129E}$ cells are different from those identified in $Pten^{WT}$ and $Pten^{Y138L}$ cells (Fig. 5H). Thus, the lipid phosphatase activity predominantly shapes the phospho-proteome in response to PTEN expression.

PTEN inhibits FRA1 via the AKT-mTOR pathway

We next sought to discover key proteins that mediate the effects of the PTEN lipid phosphatase activity, either downstream of AKT or through AKT-independent pathways. The phosphoproteomics analysis identified 143 proteins whose phosphorylation is regulated by the PTEN lipid phosphatase function in melanoma cells (Supplementary Table S2). To further prioritize these candidates, we reasoned that critical drivers of melanomagenesis may also be transcriptionally deregulated. We therefore analyzed the expression of the 143 candidates in a publicly available dataset (GSE112509) containing RNA expression data from 23 nevi and 57 melanomas (41). Seven genes exhibited significantly increased

expression in melanoma compared to nevi, indicating they may be oncogenic in melanoma (Fig. 6A). Interestingly, FOSL1, which encodes that AP-1 transcription factor FRA1, is the most upregulated gene in melanoma (fold change = 7.574) (Fig. 6A,B). Moreover, an analysis of the TCGA-SKCM dataset revealed that high expression of FOSL1 negatively correlates with the overall survival of melanoma patients (Fig. 6C).

The phosphoproteomic analysis identified five phosphosites within Fra1, two of which, Ser254 and Ser267 (corresponding to human Ser252 and Ser265), are associated with FRA1 protein stability (42). It is therefore possible that the difference in phosphopeptide abundance reflects alterations in total Fra1 protein levels. Interestingly, Fra1 protein levels are increased in 15 out of 21 mouse melanoma cell lines compared to mouse nevus, while the remaining six cell lines exhibited very low Fra1 levels (Fig. 6D). FRA1 protein levels are similarly increased in human melanoma cell lines compared to human melanocytes, and several of the cell lines exhibiting high FRA1 levels also have low or absent PTEN (Fig. 6E). We next assessed if PTEN expression influences FRA1 abundance. FOSL1 mRNA levels were unaffected by PTEN expression in both human and mouse melanoma cell lines, indicating posttranscriptional regulation of FRA1 by PTEN (Supplementary Fig. S6A). Consistent with the phosphoproteomic analysis, Ser265-phosphorylated and total FRA1 levels decreased upon wildtype PTEN expression in human and mouse melanoma cell lines (Fig. 6F), while PTEN silencing increased both phosphorylated and total FRA1 protein levels (Fig. 6F). We were unable to detect an interaction of PTEN with FRA1 by co-immunoprecipitation assays (Supplementary Fig. S6B), suggesting that FRA1 is not a direct substrate of PTEN. To characterize the signaling pathway connecting PTEN to FRA1, we firstly treated human and mouse melanoma cell lines with MK2206 and found that Ser265-phosphorylated and total FRA1 levels were decreased by the AKT inhibitor (Fig. 6G). Since mTOR is a major downstream effector of AKT, we assessed the effect of the mTORC1 inhibitor Rapamycin on FRA1 expression. mTOR inhibition reduced pSer265 and total FRA1 levels in human and mouse melanoma cell lines (Fig. 6H).

MAPK signaling increases FRA1 protein stability by phosphorylating Ser252 and Ser265 (42,43). To determine whether AKT/mTOR signaling regulates FRA1 in a similar manner, we treated mouse and human melanoma cells with the MEK inhibitor AZD6244 or Rapamycin. Notably, AZD6244 provoked a faster decrease of both phosphorylated and total FRA1 compared to Rapamycin, suggesting that the MAPK and AKT/mTOR pathways regulate FRA1 through different mechanisms (Fig. 7A). Indeed, PTEN modulation regulated AKT activity but not ERK activity, indicating that the PTEN-mediated regulation of FRA1 may be independent of the MAPK-mediated control of FRA1 stability (Fig. 6F). To further test this hypothesis, we examined if PTEN expression promotes the turnover of FRA1. To this end, we treated melanoma cells with the translation inhibitor Cycloheximide and assessed FRA1 degradation in response to PTEN expression. FRA1 degradation was not accelerated by PTEN expression (Supplementary Fig. S6C), and while active Akt^{E17K} rescued the reduction of FRA1 levels in PTEN-expressing cells, it had no effect on FRA1 turnover (Supplementary Fig. S6C). Thus, PTEN does not regulate the stability of FRA1. The mTORC1 complex is a critical regulator of protein translation and we next examined whether PTEN attenuates FRA1 protein levels by reducing its translation. Notably, following the treatment with the proteasome inhibitor MG132, Fra1 protein rapidly

accumulated in Pten^{C124S} cells but not in Pten^{WT} cells (Fig. 7B). Moreover, restoring Akt signaling with Akt^{E17K} in Pten^{WT} cells promoted the accumulation of FRA1 protein in response to MG132 treatment (Fig. 7B). Similar to Pten restoration, inhibition of mTor with Rapamycin significantly inhibited Fra1 protein accumulation in response to MG132 treatment (Fig. 7C). To further determine the translation regulation of FRA1 by the AKT/mTOR pathway, we generated a FRA1 translation reporter (FRA1-TR) consisting of 300bp of the *FRA1* 5'UTR upstream of a *GFP* cDNA and expressed this reporter in mouse and human melanoma cells. Rapamycin treatment robustly decreased GFP protein level and average GFP density expression in cells harboring the FRA1 translation reporter (Fig. 7D–F). Expression of a control *GFP* cDNA lacking the *FRA1* 5'UTR was not affected by Rapamycin (Fig. 7D). These results suggest that PTEN diminishes FRA1 translation by suppressing the AKT/mTOR-axis.

FRA1 repression mediates melanoma suppression by PTEN.

We next examined whether PTEN provokes melanoma suppression by diminishing FRA1 protein levels. To this end, we overexpressed Fra1 in melanoma cells in which Pten function was restored by expressing Pten^{WT} (Supplementary Fig. S7A). Fra1 overexpression was unable to rescue the suppressive effect of Pten on cell proliferation and low-density growth (Fig. 8A,B, Supplementary Fig. S7B). By contrast, overexpression of Fra1 partially rescued the anchorage-independent growth ability of melanoma cells expressing Pten^{WT} (Fig. 8C, Supplementary Fig. S7C). Similar to Akt^{E17K}, Fra1 fully restored cell invasion in melanoma cells expressing Pten (Fig. 8D, Supplementary Fig. S7D). Silencing of FRA1 has been shown to reduce human melanoma cell growth (44). We similarly found that silencing of FRA1 in mouse and human melanoma cells with shRNA or siRNA decreased cell invasion (Figure 8E,F, Supplementary Fig. S7E–G). Moreover, allograft transplant models demonstrated that Fra1 fully restored subcutaneous tumor growth of melanoma cells in which Pten activity was restored (Fig. 8G,H, Supplementary Fig. S3B). Thus, FRA1 expression potently overcomes most aspects of PTEN-mediated melanoma suppression that are also overcome by restoring AKT signaling. Taken together, PTEN exerts its melanoma suppressive functions at least in part by diminishing AKT-mediated FRA1 expression.

DISCUSSION

PTEN loss-of-function occurs in up to half of all malignant melanomas, and the resulting disruptions in downstream pathways may offer exploitable vulnerabilities for targeted therapies. Although drugs targeting AKT or mTOR have been developed, their routine clinical use for treating melanoma has not been realized. In fact, the underwhelming preclinical and clinical performances of these inhibitors have prompted two fundamental questions regarding PTEN-mediated melanoma suppression. First, does PTEN suppress melanoma through its lipid phosphatase activity? And second, is AKT a crucial signaling node in PTEN-deficient melanoma? Our study provides affirmative answers to these questions, demonstrating that loss of PTEN's lipid phosphatase activity promotes melanomagenesis predominantly through AKT activation. Moreover, we uncovered an AKT/mTOR/FRA1 axis that plays a key role in PTEN-mediated melanoma suppression.

It is widely assumed that the loss of PTEN promotes melanomagenesis through increased PIP_3 levels and the consequential activation of downstream signaling pathways. However, this assumption discounts the contribution of the protein phosphatase and scaffold functions of PTEN, neither of which has previously been characterized in melanoma. Our collection of murine melanoma cell lines and the ESC-GEMM platform (14,39) enabled the analysis of different PTEN functions in an otherwise PTEN-deficient background, revealing lipid phosphatase activity as the predominant melanoma suppressive function. The scaffold function retained by the $Pten^{C124S}$ mutant had no effect in vitro and in vivo, while the protein phosphatase active $Pten^{G129E}$ mutant only moderately impacted anchorage-independent growth. Besides its cytoplasmic localization, PTEN also enters the nucleus where it controls DNA damage repair, genomic integrity, transcription, and chromatin structure (45). The role of the nuclear functions of PTEN in melanoma suppression remains to be investigated. However, PTEN shifts from the nucleus to the cytoplasm in melanomagenesis (46,47) and our findings highlight PTEN-mediated control of FRA1 translation via AKT/mTOR signaling, indicating that PTEN suppresses melanomagenesis primarily in the cytoplasm.

When the PTEN lipid phosphatase activity is lost in melanoma, the resulting increase in PIP_3 levels will activate several independent signaling pathways (16). It is conceivable that these pathways work in concert to promote melanomagenesis, offering a potential explanation as to why AKT and mTOR inhibitors are not sufficient to target melanoma. However, our unbiased drug screening and phosphoproteomics approaches aimed at identifying pathways activated by the loss of PTEN lipid phosphatase activity suggested the critical importance of AKT signaling. Moreover, activated AKT was sufficient to rescue the suppression of PTEN-deficient melanoma by acute PTEN restoration. In a complementary study, Parkman et al. demonstrated that genetic silencing of all three AKT paralogs diminished the proliferation and induced cell death of PTEN-deficient melanoma cells (48). These findings support the notion that AKT is the predominant effector downstream of PIP_3, promoting melanomagenesis upon the loss of the PTEN lipid phosphatase activity.

Interestingly, we observed different potencies of AKT in overcoming PTEN-mediated melanoma suppression. While AKT only moderately rescued the growth of melanoma cells in proliferation, low density, and anchorage-independence assays, it completely rescued cell invasion in vitro and tumor growth in allograft experiments. The effects of AKT on invasion are in line with previous reports on the pro-invasive and pro-metastatic role of AKT1 in melanoma (9,10). We were unable to test the effect of PTEN and AKT on spontaneous metastasis in our study due to the rapid growth of the primary tumors in transplant models. Similarly, in our genetic BPP models, most tumors that developed were escapers in which ectopic PTEN was not expressed, precluding a meaningful analysis of the metastatic burden in these mice. While PTEN alterations occur late in melanomagenesis (1,49), the relative contribution of AKT to the metastatic spreading of PTEN-deficient melanoma remains to be investigated in more detail. While the effect of PTEN restoration on invasion and transplant tumor growth is completely dependent on inactivation of AKT, other in vitro phenotypes are likely influenced by other effector pathways. Our results using our ESC-GEMM models to restore PTEN at tumor initiation further demonstrate that PTEN suppresses the early steps of melanocyte transformation and melanoma progression, which corroborates the drastically

accelerated melanoma formation in $Braf^{V600E}$; $Pten^{null}$ mice (13). The effects of PTEN in early melanomagenesis are also dependent on its lipid phosphatase activity, but whether AKT is required at these stages remains to be determined.

Our study and the study by Parkman et al. (48) aimed to provide an answer to the question of whether AKT is an inadequate therapeutic target in PTEN-deficient melanoma or if AKT inhibitors lack the efficacy to elicit anti-melanoma effects. Our results show AKT-independent pathways contribute to melanoma proliferation in vitro, while in vivo tumor growth in transplant models completely relies on AKT. Parkman et al. demonstrate that depletion of all three AKT paralogs kills melanoma cells and outperforms current AKT inhibitors (48). These findings suggest that AKT inhibitors having improved potency may perform better in the clinic. By contrast, we show that the AKT inhibitor MK2206 fully mimics the effect of PTEN restoration on cell invasion, an in vitro phenotype that is entirely dependent on AKT. Thus, whether current AKT inhibitors are simply not potent enough is difficult to reconcile, but regardless, their lack of efficacy in the clinic calls for better and improved treatment strategies. The efficacy of any future AKT inhibitors must be determined in assays that rely predominantly on AKT activity, while the effectiveness of these drugs is best evaluated using in vivo models that encompass the full spectrum of PTEN loss-induced downstream effectors. However, whether pan-AKT inhibition that recapitulates the genetic silencing of all three AKT paralogs while eliciting low toxicity can be accomplished is questionable. Alternative treatment strategies for PTEN-deficient melanomas therefore need to be devised. One approach could be the combinatorial inhibition of AKT and parallel PIP_3-dependent pathways that contribute to melanomagenesis. One such parallel pathway could be the SGK pathway, which has previously been implicated in melanoma (17). Indeed, Parkman et al. identified a compensatory increase in SGK1 expression upon pan-AKT silencing (48). This suggests that SGK1 represents a bypass mechanism that could explain why AKT inhibition has limited effects on proliferation. However, why melanoma cell invasion relies entirely on AKT without contribution by SGK1 or other parallel pathways remains to be determined. Nevertheless, Parkman et al. demonstrated superior melanoma cell killing by combined AKT and SGK inhibition (48), showing that targeting of these parallel pathways is a viable therapeutic strategy.

In addition to parallel pathways, downstream effectors of AKT may prove useful for combination therapy strategies. We aimed to identify such downstream effectors through phosphoproteomics, which revealed 143 candidate proteins that are potentially regulated by the PTEN lipid phosphatase activity. Only 18 of these proteins are thought to participate in canonical PI3K/AKT signaling, while 101 proteins have never or rarely (<10 studies) been associated with AKT signaling. Our strategy to prioritize candidates by analyzing their expression in melanoma revealed the AP-1 transcription factor FRA1 as the top candidate. We found remarkably elevated FRA1 protein abundance in murine and human melanoma cell lines. However, these increases also occurred in some cell lines having intact PTEN, suggesting that FRA1 is regulated by additional pathways. Indeed, ERK and PKC phosphorylate FRA1, preventing its proteasomal degradation (42,43). Our results instead point toward translational regulation of FRA1 via AKT and mTOR, a mechanism that has previously been suggested (50). Thus, multiple pathways converge on FRA1,

enhancing FRA1 protein abundance by regulating translation and turnover. FRA1 is capable of transforming melanocytes in vitro leading to a reprogrammed cell state that even in the absence of continuous FRA1 expression enables tumor formation in transplant models (44). Whether FRA1 contributes to spontaneous melanoma formation in genetic mouse models and what aspects of melanomagenesis are affected by FRA1 remains to be determined. We showed that FRA1 overexpression recapitulates the effects of AKT in overcoming PTEN-mediated melanoma suppression, specifically invasion and tumor growth. FRA1 expression has also previously been associated with an invasive phenotype in melanoma cell lines (44). These findings suggest that FRA1 is a key AKT effector expected to play important roles in the same steps of melanomagenesis as AKT. Interestingly, FRA1 upregulation is critical for the survival of MAPK inhibitor-addicted melanoma cells (51,52), indicating that FRA1 targeting may forestall or overcome acquired resistance to BRAF and MEK inhibitors. While therapeutic targeting of FRA1 will need innovative approaches (53), early efforts with compounds that target the ERK-FRA1 interface have resulted in diminished FRA1 protein levels and enhanced apoptosis of melanoma cells (54). Taken together, not only does the discovery of the AKT/mTOR/FRA1 axis add to our understanding of AKT-mediated melanomagenesis, but it may also offer new opportunities for targeting PTEN-deficient melanoma.

Supplementary Material

Refer to Web version on PubMed Central for supplementary material.

ACKNOWLEDGMENTS

We are grateful to Karreth lab members for helpful discussions. F. A. Karreth was supported by a Miles for Moffitt Award, a Harry J. Lloyd Charitable Trust Career Development Award, and a Bankhead-Coley Grant (21B04) from the Florida Department of Health. This work was also supported by the Gene Targeting Core, the Proteomics Core, and the Biostatistics and Bioinformatics Shared Resource, which are funded in part by Moffitt's Cancer Center Support Grant (P30CA076292).

REFERENCES

1. Shain AH, Joseph NM, Yu R, Benhamida J, Liu S, Prow T, et al. Genomic and Transcriptomic Analysis Reveals Incremental Disruption of Key Signaling Pathways during Melanoma Evolution. Cancer cell. 2018;34:45–55.e4. [PubMed: 29990500]
2. Network CGA. Genomic Classification of Cutaneous Melanoma. Cell. 2015;161:1681–96. [PubMed: 26091043]
3. Manning BD, Toker A. AKT/PKB Signaling: Navigating the Network. Cell. 2017;169:381–405. [PubMed: 28431241]
4. Fruman DA, Chiu H, Hopkins BD, Bagrodia S, Cantley LC, Abraham RT. The PI3K Pathway in Human Disease. Cell. 2017;170:605–35. [PubMed: 28802037]
5. Thorpe LM, Yuzugullu H, Zhao JJ. PI3K in cancer: divergent roles of isoforms, modes of activation and therapeutic targeting. Nat Rev Cancer. 2015;15:7–24. [PubMed: 25533673]
6. Song MS, Salmena L, Pandolfi PP. The functions and regulation of the PTEN tumour suppressor. Nature reviews Molecular cell biology. 2012;13:283–96. [PubMed: 22473468]
7. Lee Y-R, Chen M, Pandolfi PP. The functions and regulation of the PTEN tumour suppressor: new modes and prospects. Nat Rev Mol Cell Bio. 2018;19:547–62. [PubMed: 29858604]
8. Zhang T, Dutton-Regester K, Brown KM, Hayward NK. The genomic landscape of cutaneous melanoma. Pigm Cell Melanoma R. 2016;29:266–83.

9. Cho JH, Robinson JP, Arave RA, Burnett WJ, Kircher DA, Chen G, et al. AKT1 Activation Promotes Development of Melanoma Metastases. Cell reports. 2015;13:898–905. [PubMed: 26565903]
10. Kircher DA, Trombetti KA, Silvis MR, Parkman GL, Fischer GM, Angel SN, et al. AKT1E17K Activates Focal Adhesion Kinase and Promotes Melanoma Brain Metastasis. Mol Cancer Res. 2019;17:1787–800. [PubMed: 31138602]
11. Deuker MM, Durban VM, Phillips WA, McMahon M. PI3′-Kinase Inhibition Forestalls the Onset of MEK1/2 Inhibitor Resistance in BRAF-Mutated Melanoma. Cancer Discov. 2015;5:143–53. [PubMed: 25472943]
12. Durban VM, Deuker MM, Bosenberg MW, Phillips W, McMahon M. Differential AKT dependency displayed by mouse models of BRAFV600E-initiated melanoma. The Journal of clinical investigation. 2013;123:5104–18. [PubMed: 24200692]
13. Dankort D, Curley DP, Cartlidge RA, Nelson B, Karnezis AN, Damsky WE, et al. Braf(V600E) cooperates with Pten loss to induce metastatic melanoma. Nature genetics. 2009;41:544–52. [PubMed: 19282848]
14. Bok I, Vera O, Xu X, Jasani N, Nakamura K, Reff J, et al. A versatile ES cell-based melanoma mouse modeling platform. Cancer research. 2019;80:canres.2924.2019–921.
15. Silva JM, Bulman C, McMahon M. BRAFV600E Cooperates with PI3K Signaling, Independent of AKT, to Regulate Melanoma Cell Proliferation. Mol Cancer Res. 2014;12:447–63. [PubMed: 24425783]
16. Lien EC, Dibble CC, Toker A. PI3K signaling in cancer: beyond AKT. Curr Opin Cell Biol. 2017;45:62–71. [PubMed: 28343126]
17. Scortegagna M, Lau E, Zhang T, Feng Y, Sereduk C, Yin H, et al. PDK1 and SGK3 Contribute to the Growth of BRAF-Mutant Melanomas and Are Potential Therapeutic Targets. Cancer research. 2015;75:1399–412. [PubMed: 25712345]
18. Scortegagna M, Ruller C, Feng Y, Lazova R, Kluger H, Li J-L, et al. Genetic inactivation or pharmacological inhibition of Pdk1 delays development and inhibits metastasis of Braf(V600E)::Pten(−/−) melanoma. Oncogene. 2014;33:4330–9. [PubMed: 24037523]
19. Li J, Yen C, Liaw D, Podsypanina K, Bose S, Wang SI, et al. PTEN, a Putative Protein Tyrosine Phosphatase Gene Mutated in Human Brain, Breast, and Prostate Cancer. Science. 1997;275:1943–7. [PubMed: 9072974]
20. Myers MP, Stolarov JP, Eng C, Li J, Wang SI, Wigler MH, et al. P-TEN, the tumor suppressor from human chromosome 10q23, is a dual-specificity phosphatase. Proc National Acad Sci. 1997;94:9052–7.
21. Tamura M, Gu J, Matsumoto K, Aota S, Parsons R, Yamada KM. Inhibition of Cell Migration, Spreading, and Focal Adhesions by Tumor Suppressor PTEN. Science. 1998;280:1614–7. [PubMed: 9616126]
22. Dey N, Crosswell HE, De P, Parsons R, Peng Q, Su JD, et al. The Protein Phosphatase Activity of PTEN Regulates Src Family Kinases and Controls Glioma Migration. Cancer Res. 2008;68:1862–71. [PubMed: 18339867]
23. Shi Y, Wang J, Chandarlapaty S, Cross J, Thompson C, Rosen N, et al. PTEN is a protein tyrosine phosphatase for IRS1. Nat Struct Mol Biol. 2014;21:522–7. [PubMed: 24814346]
24. Qian X, Li X, Shi Z, Xia Y, Cai Q, Xu D, et al. PTEN Suppresses Glycolysis by Dephosphorylating and Inhibiting Autophosphorylated PGK1. Mol Cell. 2019;76:516–527.e7. [PubMed: 31492635]
25. Shinde SR, Maddika S. PTEN modulates EGFR late endocytic trafficking and degradation by dephosphorylating Rab7. Nat Commun. 2016;7:10689. [PubMed: 26869029]
26. Yip HYK, Chee A, Ang C-S, Shin S-Y, Ooms LM, Mohammadi Z, et al. Control of Glucocorticoid Receptor Levels by PTEN Establishes a Failsafe Mechanism for Tumor Suppression. Mol Cell. 2020;80:279–295.e8. [PubMed: 33065020]
27. Tibarewal P, Zilidis G, Spinelli L, Schurch N, Maccario H, Gray A, et al. PTEN Protein Phosphatase Activity Correlates with Control of Gene Expression and Invasion, a Tumor-Suppressing Phenotype, But Not with AKT Activity. Sci Signal. 2012;5:ra18.

28. Gildea JJ, Herlevsen M, Harding MA, Gulding KM, Moskaluk CA, Frierson HF, et al. PTEN can inhibit in vitro organotypic and in vivo orthotopic invasion of human bladder cancer cells even in the absence of its lipid phosphatase activity. Oncogene. 2004;23:6788–97. [PubMed: 15273733]
29. Raftopoulou M, Etienne-Manneville S, Self A, Nicholls S, Hall A. Regulation of Cell Migration by the C2 Domain of the Tumor Suppressor PTEN. Science. 2004;303:1179–81. [PubMed: 14976311]
30. Yu Y, Dai M, Huang L, Chen W, Yu E, Mendoza A, et al. PTEN phosphatase inhibits metastasis by negatively regulating the Entpd5/IGF1R pathway through ATF6. Iscience. 2023;26:106070. [PubMed: 36824269]
31. Kuchay S, Giorgi C, Simoneschi D, Pagan J, Missiroli S, Saraf A, et al. PTEN counteracts FBXL2 to promote IP3R3- and Ca2+-mediated apoptosis limiting tumour growth. Nature. 2017;546:554–8. [PubMed: 28614300]
32. Zhao D, Lu X, Wang G, Lan Z, Liao W, Li J, et al. Synthetic essentiality of chromatin remodelling factor CHD1 in PTEN-deficient cancer. Nature. 2017;542:484–8. [PubMed: 28166537]
33. Fang B, Izumi V, Rix LLR, Welsh E, Pike I, Reuther GW, et al. Lowering Sample Requirements to Study Tyrosine Kinase Signaling Using Phosphoproteomics with the TMT Calibrator Approach. Proteomics. 2020;20:e2000116. [PubMed: 32865326]
34. Welsh EA, Eschrich SA, Berglund AE, Fenstermacher DA. Iterative rank-order normalization of gene expression microarray data. Bmc Bioinformatics. 2013;14:153. [PubMed: 23647742]
35. Chen EY, Tan CM, Kou Y, Duan Q, Wang Z, Meirelles GV, et al. Enrichr: interactive and collaborative HTML5 gene list enrichment analysis tool. BMC Bioinform. 2013;14:128.
36. Kuleshov MV, Jones MR, Rouillard AD, Fernandez NF, Duan Q, Wang Z, et al. Enrichr: a comprehensive gene set enrichment analysis web server 2016 update. Nucleic Acids Res. 2016;44:W90–7. [PubMed: 27141961]
37. Subramanian A, Tamayo P, Mootha VK, Mukherjee S, Ebert BL, Gillette MA, et al. Gene set enrichment analysis: a knowledge-based approach for interpreting genome-wide expression profiles. Proceedings of the National Academy of Sciences of the United States of America. 2005;102:15545–50. [PubMed: 16199517]
38. Tang Z, Li C, Kang B, Gao G, Li C, Zhang Z. GEPIA: a web server for cancer and normal gene expression profiling and interactive analyses. Nucleic Acids Res. 2017;45:W98–102. [PubMed: 28407145]
39. Bok I, Angarita A, Douglass SM, Weeraratna AT, Karreth FA. A series of BRAF- and NRAS-driven murine melanoma cell lines with inducible gene modulation capabilities. Jid Innovations. 2021;100076. [PubMed: 35146482]
40. Sumi NJ, Ctortecka C, Hu Q, Bryant AT, Fang B, Rix LLR, et al. Divergent Polypharmacology-Driven Cellular Activity of Structurally Similar Multi-Kinase Inhibitors through Cumulative Effects on Individual Targets. Cell chemical biology. 2019;26:1240–1252.e11. [PubMed: 31257184]
41. Kunz M, Löffler-Wirth H, Dannemann M, Willscher E, Doose G, Kelso J, et al. RNA-seq analysis identifies different transcriptomic types and developmental trajectories of primary melanomas. Oncogene. 2018;37:6136–51. [PubMed: 29995873]
42. Basbous J, Chalbos D, Hipskind R, Jariel-Encontre I, Piechaczyk M. Ubiquitin-Independent Proteasomal Degradation of Fra-1 Is Antagonized by Erk1/2 Pathway-Mediated Phosphorylation of a Unique C-Terminal Destabilizer. Mol Cell Biol. 2007;27:3936–50. [PubMed: 17371847]
43. Belguise K, Milord S, Galtier F, Moquet-Torcy G, Piechaczyk M, Chalbos D. The PKCθ pathway participates in the aberrant accumulation of Fra-1 protein in invasive ER-negative breast cancer cells. Oncogene. 2012;31:4889–97. [PubMed: 22286759]
44. Maurus K, Hufnagel A, Geiger F, Graf S, Berking C, Heinemann A, et al. The AP-1 transcription factor FOSL1 causes melanocyte reprogramming and transformation. Oncogene. 2017;36:5110–21. [PubMed: 28481878]
45. Langdon CG. Nuclear PTEN's Functions in Suppressing Tumorigenesis: Implications for Rare Cancers. Biomol. 2023;13:259.
46. Tsao H, Mihm MC, Sheehan C. PTEN expression in normal skin, acquired melanocytic nevi, and cutaneous melanoma. J Am Acad Dermatol. 2003;49:865–72. [PubMed: 14576666]

47. Whiteman DC, Zhou X, Cummings MC, Pavey S, Hayward NK, Eng C. Nuclear PTEN expression and clinicopathologic features in a population-based series of primary cutaneous melanoma. Int J Cancer. 2002;99:63–7. [PubMed: 11948493]

48. Parkman GL, Turapov T, Kircher DA, Burnett WJ, Stehn CM, O'Toole K, et al. Genetic silencing of AKT induces melanoma cell death via mTOR suppression. Mol cancer Ther. 2023;

49. Cabrita R, Mitra S, Sanna A, Ekedahl H, Lövgren K, Olsson H, et al. The Role of PTEN Loss in Immune Escape, Melanoma Prognosis and Therapy Response. Cancers. 2020;12:742. [PubMed: 32245160]

50. Gu X, Yu JJ, Ilter D, Blenis N, Henske EP, Blenis J. Integration of mTOR and estrogen–ERK2 signaling in lymphangioleiomyomatosis pathogenesis. Proc Natl Acad Sci. 2013;110:14960–5. [PubMed: 23983265]

51. Hong A, Moriceau G, Sun L, Lomeli S, Piva M, Damoiseaux R, et al. Exploiting drug addiction mechanisms to select against MAPKi-resistant melanoma. Cancer Discov. 2017;8:CD-17–0682.

52. Kong X, Kuilman T, Shahrabi A, Boshuizen J, Kemper K, Song J-Y, et al. Cancer drug addiction is relayed by an ERK2-dependent phenotype switch. Nature. 2017;550:270–4. [PubMed: 28976960]

53. Casalino L, Talotta F, Cimmino A, Verde P. The Fra-1/AP-1 Oncoprotein: From the "Undruggable" Transcription Factor to Therapeutic Targeting. Cancers. 2022;14:1480. [PubMed: 35326630]

54. Samadani R, Zhang J, Brophy A, Oashi T, Priyakumar UD, Raman EP, et al. Small-molecule inhibitors of ERK-mediated immediate early gene expression and proliferation of melanoma cells expressing mutated BRaf. Biochem J. 2015;467:425–38. [PubMed: 25695333]

SIGNIFICANCE

PTEN suppresses melanoma predominantly through its lipid phosphatase function, which when lost elevates FRA1 levels through AKT/mTOR signaling to promote several aspects of melanomagenesis.

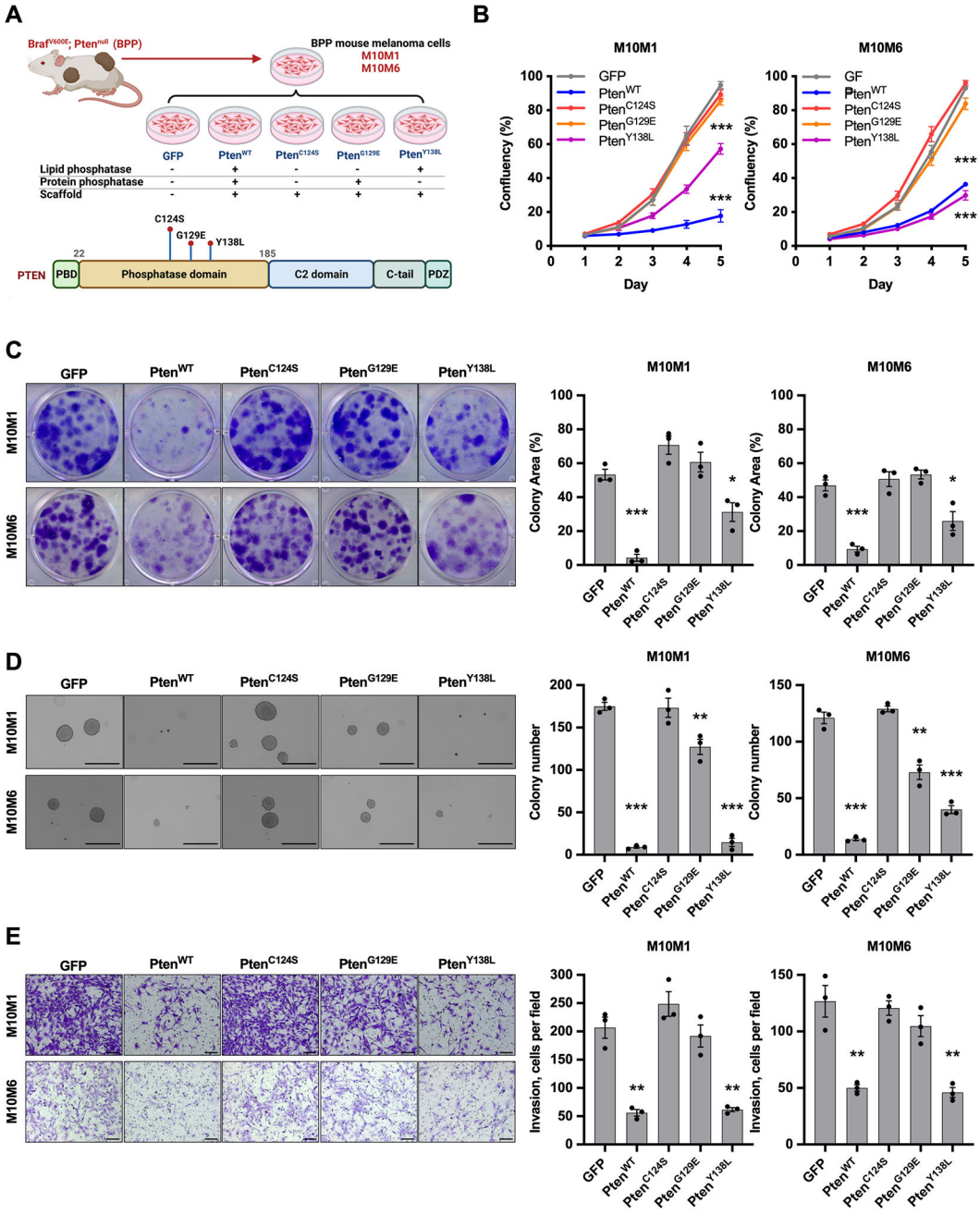

Figure 1. Comparison of different PTEN functions in melanoma suppression in vitro.

A, Schematic diagram depicting the generation of mouse melanoma cell lines harboring inducible expression constructs of different PTEN mutants (created with BioRender.com). **B,** Proliferation as measured by relative confluence of M10M6 and M10M1 cells expressing Pten constructs. **C,** Representative images (left) and quantification of percentage occupied area (right) of low-density colony formation assays of M10M6 and M10M1 cells expressing Pten constructs. **D,** Representative images (left) and quantification of colony number (right) of anchorage-independent growth agar assays of M10M6 and M10M1 cells expressing Pten constructs. Scale bars = 400μm. **E,** Representative images (left) and quantification of cell

numbers (right) of transwell invasion assays of M10M6 and M10M1 cells expressing Pten constructs. Scale bars = 100μm. Mean ± SEM are shown in (B-E). Data are analyzed with Student's unpaired *t* test, * P<0.05, ** P<0.01, *** P<0.001.

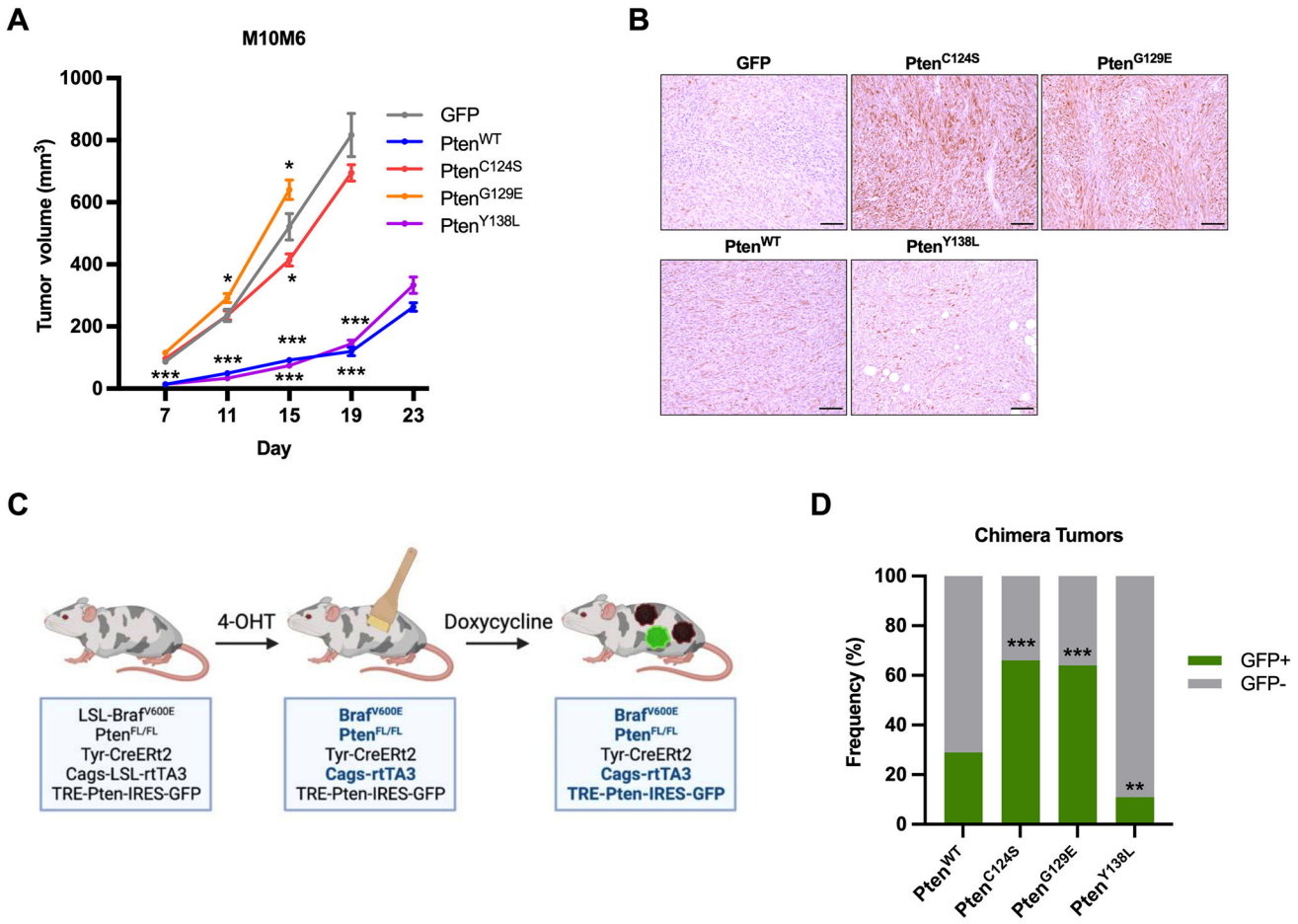

Figure 2. Lipid phosphatase activity is essential for PTEN to suppress melanoma in vivo.

A, M10M6 melanoma cells expressing Pten constructs were subcutaneously injected into NSG mice (n=10). Mice were fed chow containing 200 mg/kg Doxycycline to induce the expression of Pten mutant constructs. Tumor volumes were measured every 4 days. Tumor volumes are shown as mean ± SEM. Data are analyzed with Student's unpaired *t* test, * P<0.05, ** P<0.01, *** P<0.001. **B,** Representative images of Pten immunohistochemistry of Pten-restored tumors shown in (A). Scale bars = 100μm. **C,** Schematic diagram of the ESC-GEMMs where Pten-IRES-GFP constructs are expressed in the $Braf^{V600E}$; $Pten^{null}$ (BPP) mouse melanoma model. **(D)** Melanomas were isolated and GFP expression was detected as a surrogate for ectopic Pten expression. The percentages of GFP+ and GFP- tumors in the different Pten cohorts are shown. Data are analyzed with Chi-square test. * P<0.05, ** P<0.01, *** P<0.001.

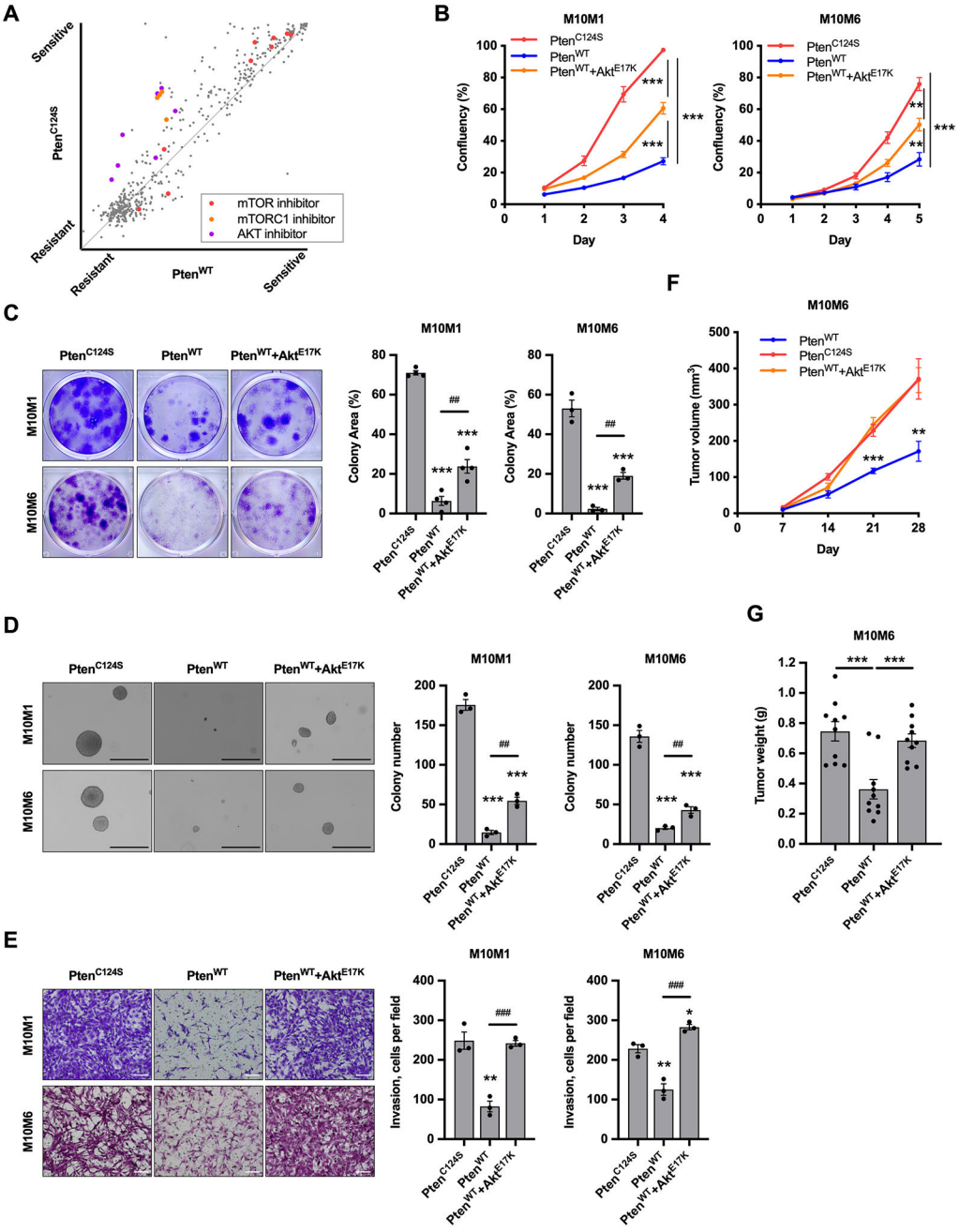

Figure 3. AKT reactivation partially abrogates melanoma suppression by PTEN.

A, M10M6 cells having Pten^{WT} or phosphatase deficient Pten^{C124S} were subjected to a small molecule inhibitor library screen containing 500 inhibitors. The sensitivity of each inhibitor towards Pten^{WT} and Pten^{C124S} cells is calculated by comparing cell viability of inhibitor treatment to DMSO control (see Materials and Methods) and plotted. **B,** Proliferation as measured by relative confluence of M10M6 and M10M1 cells expressing Pten^{WT}, Pten^{C124S}, or wildtype Pten together with constitutively activated Akt (Pten^{WT}+Akt^{E17K}). **C,** Representative images (left) and quantification of percentage occupied area (right) of low-density colony formation assays of M10M6 and M10M1

cells expressing $Pten^{WT}$, $Pten^{C124S}$, or $Pten^{WT}$+Akt^{E17K}. **D,** Representative images (left) and quantification of colony number (right) of anchorage-independent growth assays of M10M6 and M10M1 cells expressing $Pten^{WT}$, $Pten^{C124S}$, or $Pten^{WT}$+Akt^{E17K}. Scale bars = 400μm. **E,** Representative images (left) and quantification of cell numbers (right) of transwell invasion assays of M10M6 and M10M1 cells expressing $Pten^{WT}$, $Pten^{C124S}$, or $Pten^{WT}$+Akt^{E17K}. Scale bars = 100μm. **F-G,** M10M6 cells expressing $Pten^{WT}$, $Pten^{C124S}$, or $Pten^{WT}$+Akt^{E17K} were subcutaneously injected into NSG mice (n=10). Mice were fed chow containing 200 mg/kg Doxycycline to induce expression of Pten constructs. Tumor volumes were measured every 3 days. The curves of tumor volume **(F)** and the tumor weight at the end point **G,** are shown. Mean ± SEM are shown in (B-G). Data are analyzed with Student's unpaired *t* test, * P<0.05, ** P<0.01, *** P<0.001, $^{\#\#}$ P<0.01, $^{\#\#\#}$ P<0.001.

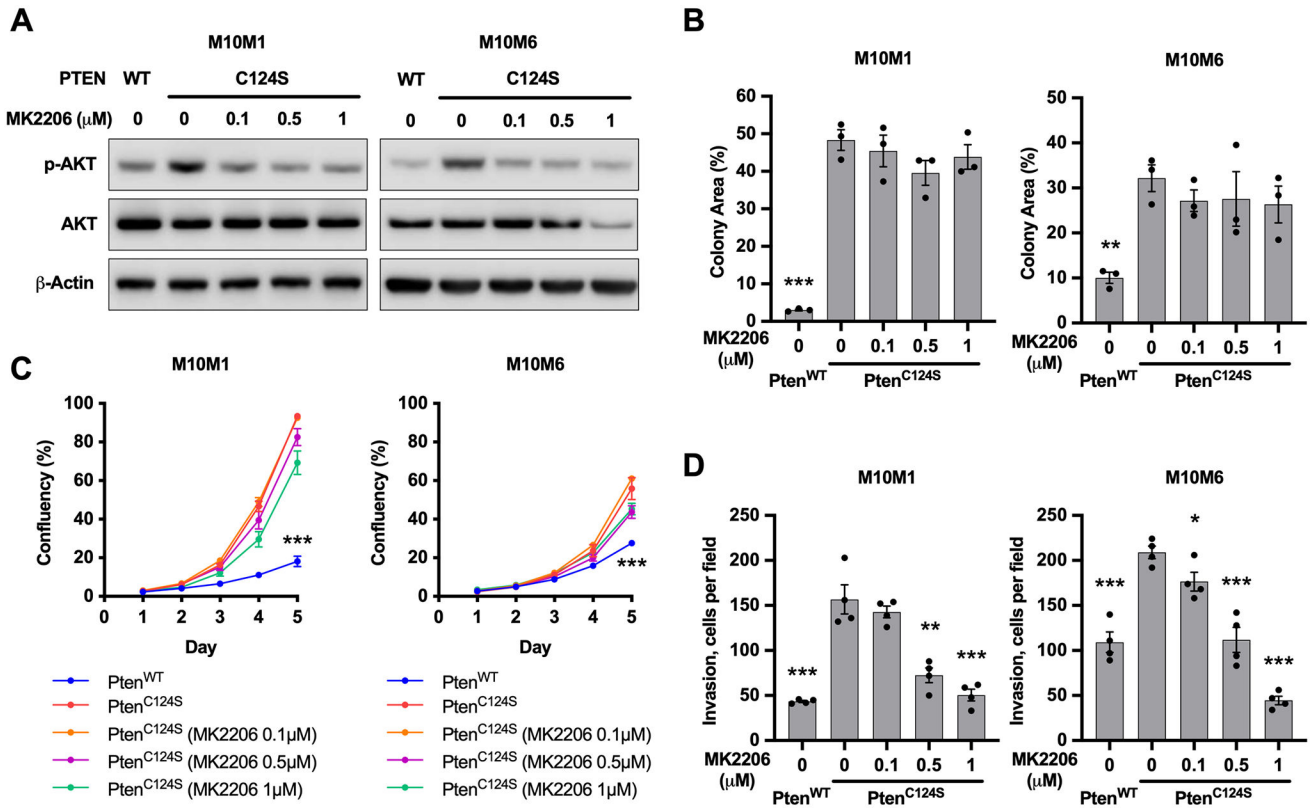

Figure 4. Comparison of tumor suppressive effects of AKT inhibitor vs. PTEN restoration.

A, Western blot showing the changes of Akt activity in M10M1 and M10M6 melanoma cells expressing $Pten^{WT}$ or $Pten^{C124S}$ and treated with the AKT inhibitor MK2206. p-Akt (Ser473), pan-Akt, p-S6K (Thr389), S6K, and β-Actin were detected. **B,** Proliferation as measured by relative confluence of M10M6 and M10M1 cells expressing $Pten^{WT}$ or $Pten^{C124S}$ and treated with the AKT inhibitor MK2206. **C,** Quantification of percentage occupied area of low-density colony formation assays of M10M6 and M10M1 cells expressing $Pten^{WT}$ or $Pten^{C124S}$ and treated with the AKT inhibitor MK2206. **D,** Quantification of cell numbers of transwell invasion assays of M10M6 and M10M1 cells expressing $Pten^{WT}$ or $Pten^{C124S}$ and treated with the AKT inhibitor MK2206. Mean ± SEM are shown in (B-D). Data are analyzed with Student's unpaired *t* test, * P<0.05, ** P<0.01, *** P<0.001

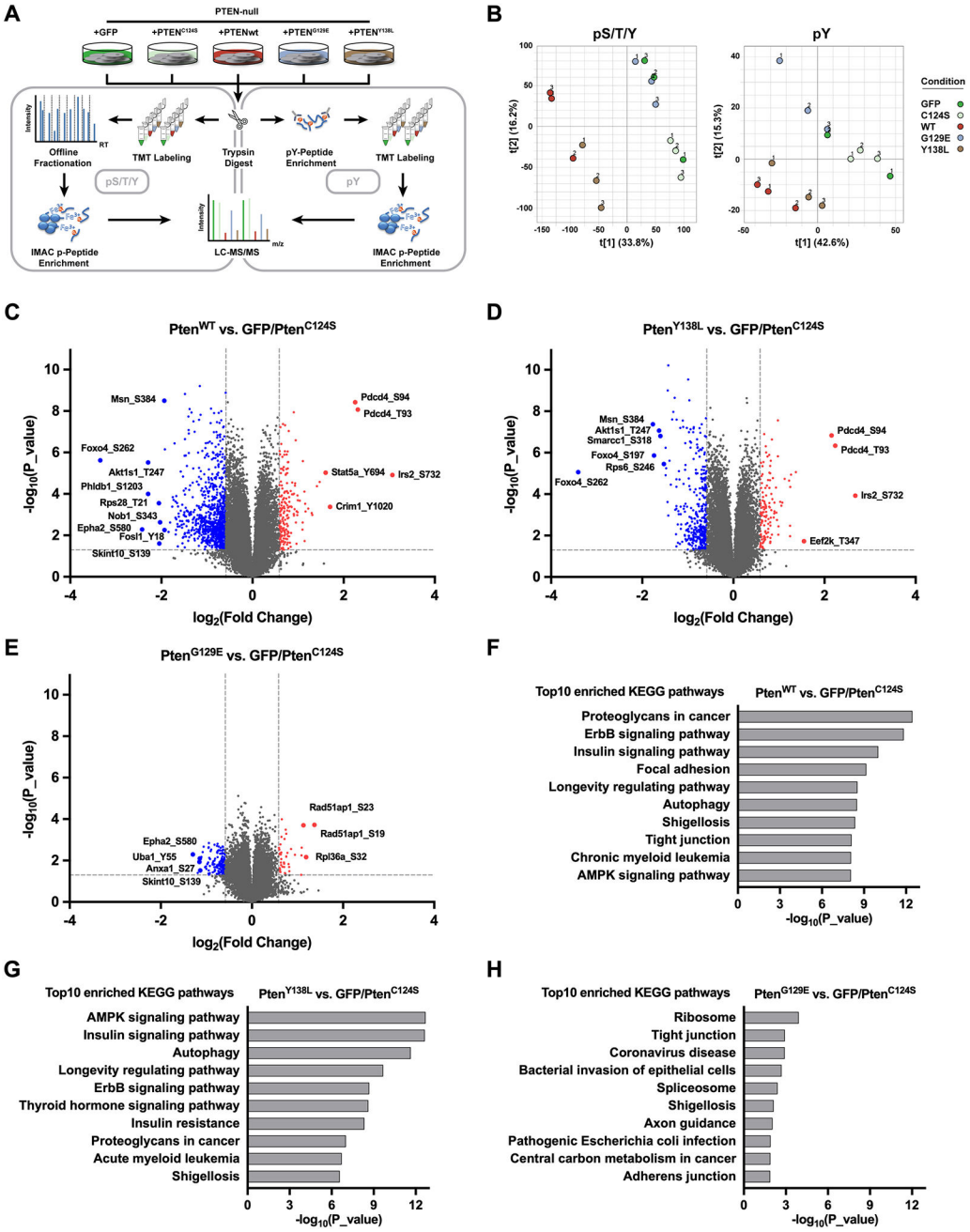

Figure 5. Quantitative global and Tyrosine phosphoproteomics analysis of network-wide signaling effects of PTEN lipid phosphatase and protein phosphatase activities.

A, Schematic of quantitative global (pS/T/Y) and Tyrosine (pY) phosphoproteomics. **B,** Principal Component Analysis of pS/T/Y (left panel) and pY (right panel) phosphoproteomics data showing all biological replicates for each condition on the first two components. **C-E,** Volcano plots indicating phosphorylation ratios of pS/T/Y and pY peptides between Pten^{WT} vs Pten^{C124S}/GFP (C), Pten^{Y138L} vs Pten^{C124S}/GFP (D), and Pten^{G129E} vs Pten^{C124S}/GFP (E). **F-H,** KEGG pathway analysis of differentially phosphorylated proteins from Pten^{WT} vs Pten^{C124S}/GFP (F), Pten^{Y138L} vs Pten^{C124S}/GFP

(G), and Pten^{G129E} vs Pten^{C124S}/GFP (H) using Enrichr. Displayed are the top 10 enriched pathways ranked by P-value.

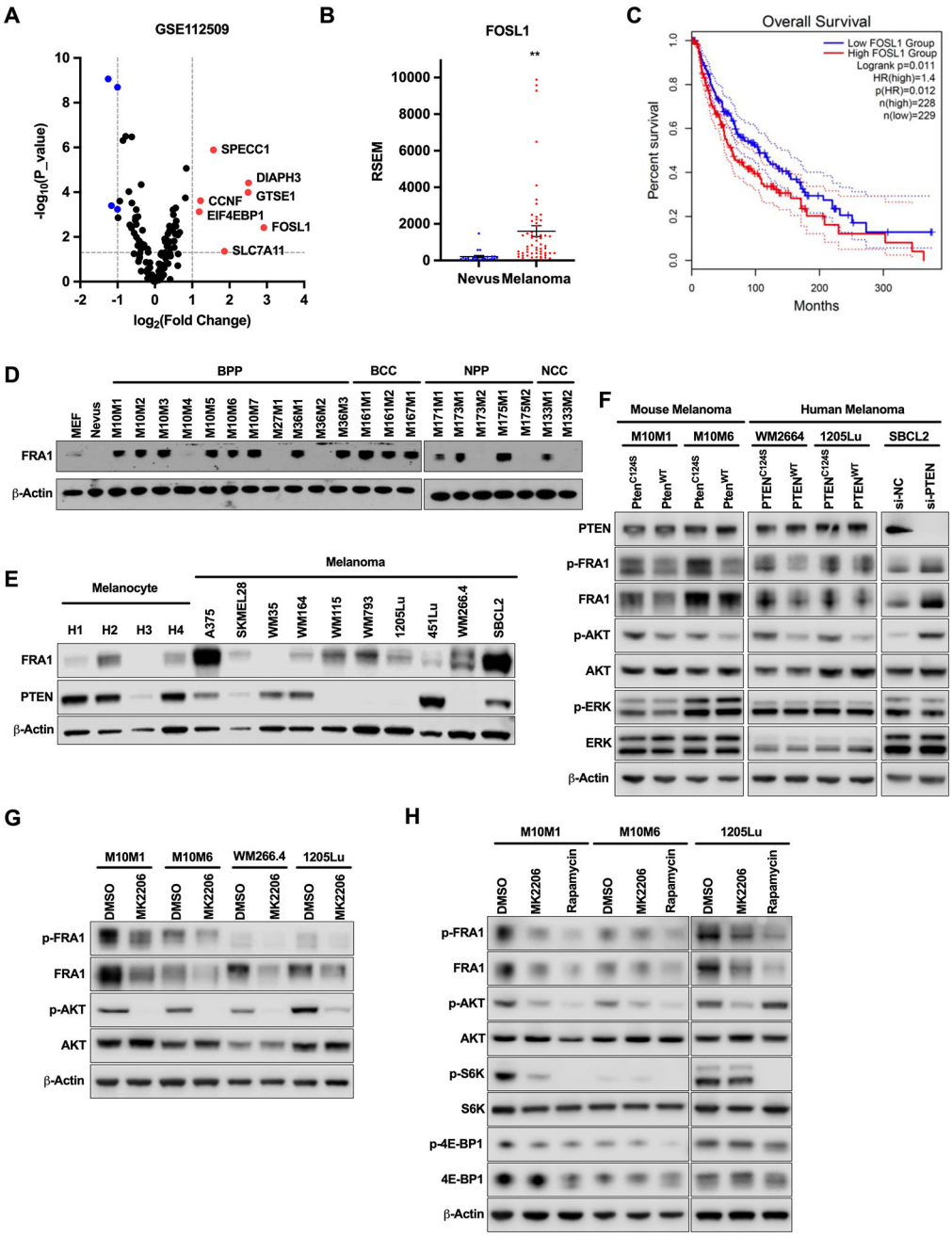

Figure 6. FRA1 is suppressed by PTEN through AKT-mTOR signaling.

A, 143 proteins were identified as potential targets of PTEN lipid phosphatase activity (see Table S2) and their differential mRNA expression between melanoma and nevi was analyzed in the GSE112509 dataset and shown as volcano plot. P-value <0.05 and fold-change >2 were used as thresholds. **B,** Expression of *FOSL1* in nevi and melanoma samples in the GSE112509 dataset. **C,** Overall survival curve of melanoma patients with high or low FRA1 expression from TCGA. **D-E,** Western blot analysis of FRA1 protein level in mouse nevus and melanoma cells (D) and in human melanocytes and melanoma cells (E). FRA1, PTEN, and β-Actin were detected. **F,** Western blot analysis of FRA1 in mouse and human

melanoma cells expressing $Pten^{WT}$ or $Pten^{C124S}$, and of human melanoma cells in which PTEN is silenced. FRA1, p-FRA1 (Ser265), pan-AKT, p-AKT (Ser473), ERK1/2, p-ERK1/2 (Thr202/Tyr204), and β-Actin were detected. **G,** Western blot analysis of FRA1 in mouse and human melanoma cells treated with the AKT inhibitor MK2206. FRA1, p-FRA1 (Ser265), pan-AKT, p-AKT (Ser473), and β-Actin were detected. **H,** Western blot analysis of FRA1 expression in mouse and human melanoma cells treated with the AKT inhibitor MK2206 or the mTOR inhibitor Rapamycin. FRA1, p-FRA1 (Ser265), pan-AKT, p-AKT (Ser473), S6K, p-S6K (Thr389), 4E-BP1, p-4E-BP1 (Ser65) and β-Actin were detected.

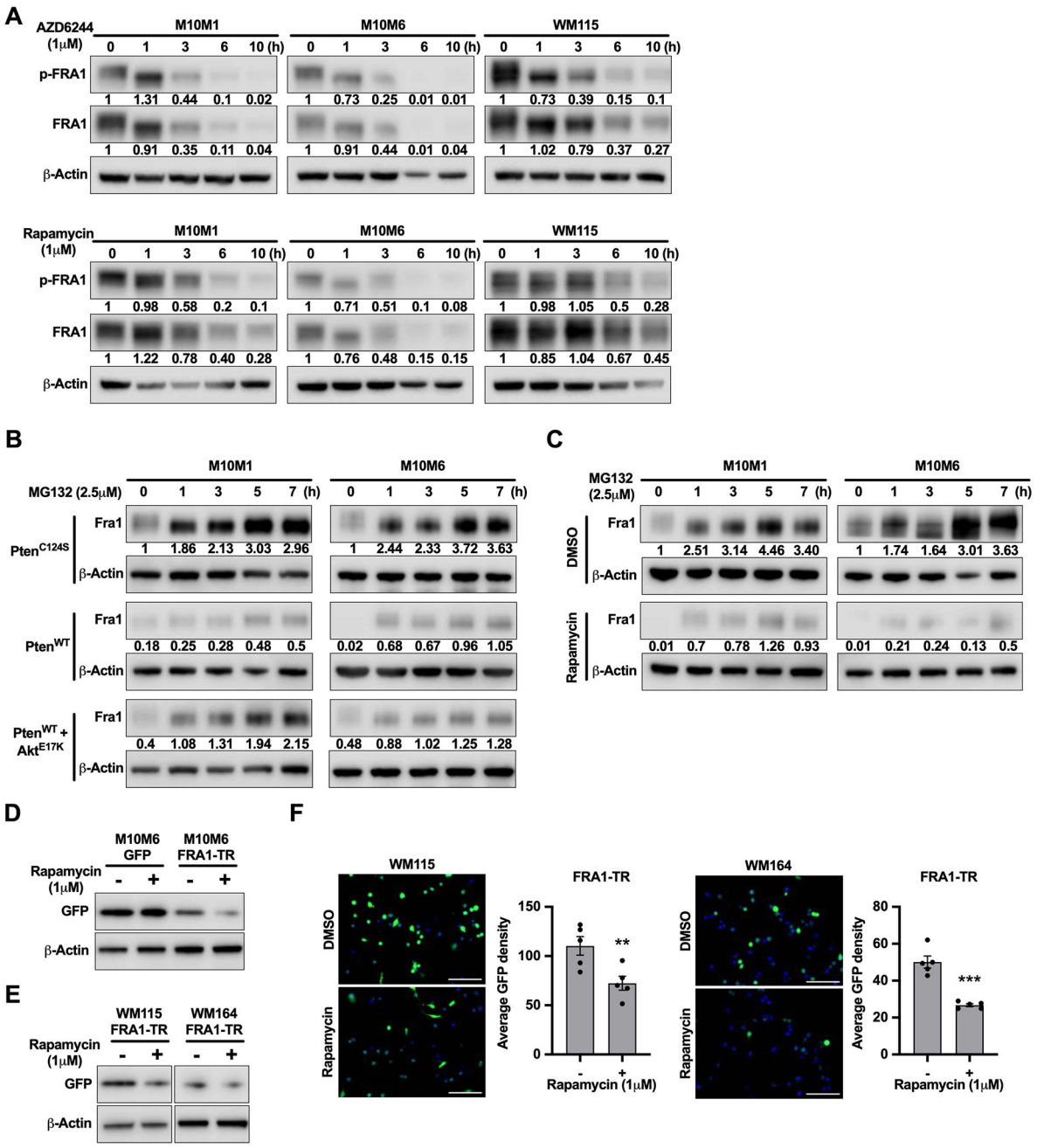

Figure 7. mTOR signaling regulates FRA1 translation.

A, Western blot analysis of FRA1 protein levels in melanoma cells treated with MEK inhibitor AZD6244 or mTOR inhibitor Rapamycin for the indicated time points. p-FRA1 (Ser265), FRA1 and β-Actin were detected. **B-C,** M10M1 and M10M6 cells expressing $Pten^{WT}$, $Pten^{C124S}$, or $Pten^{WT}$+Akt^{E17K} (B), and M10M1 and M10M6 cells treated with DMSO or Rapamycin (C), were treated with proteasome inhibitor MG132. Western blot analysis of Fra1 protein levels in melanoma cells treated with MG132 for the indicated time points are shown. **D,** M10M6 cells expressing a FRA1-translation-reporter (FRA1-TR) or GFP control were treated with Rapamycin. Western blot analysis of GFP protein levels

is shown. **E-F,** 1205Lu and WM266.4 cells expressing a FRA1-translation-reporter (FRA1-TR) were treated with DMSO or Rapamycin. Western blot analysis of GFP protein levels is shown (E). Representative fluorescent images of GFP (green) and Hoechst (blue), and quantification of average GFP density of expression is shown (F). Scale bars = 100μm.

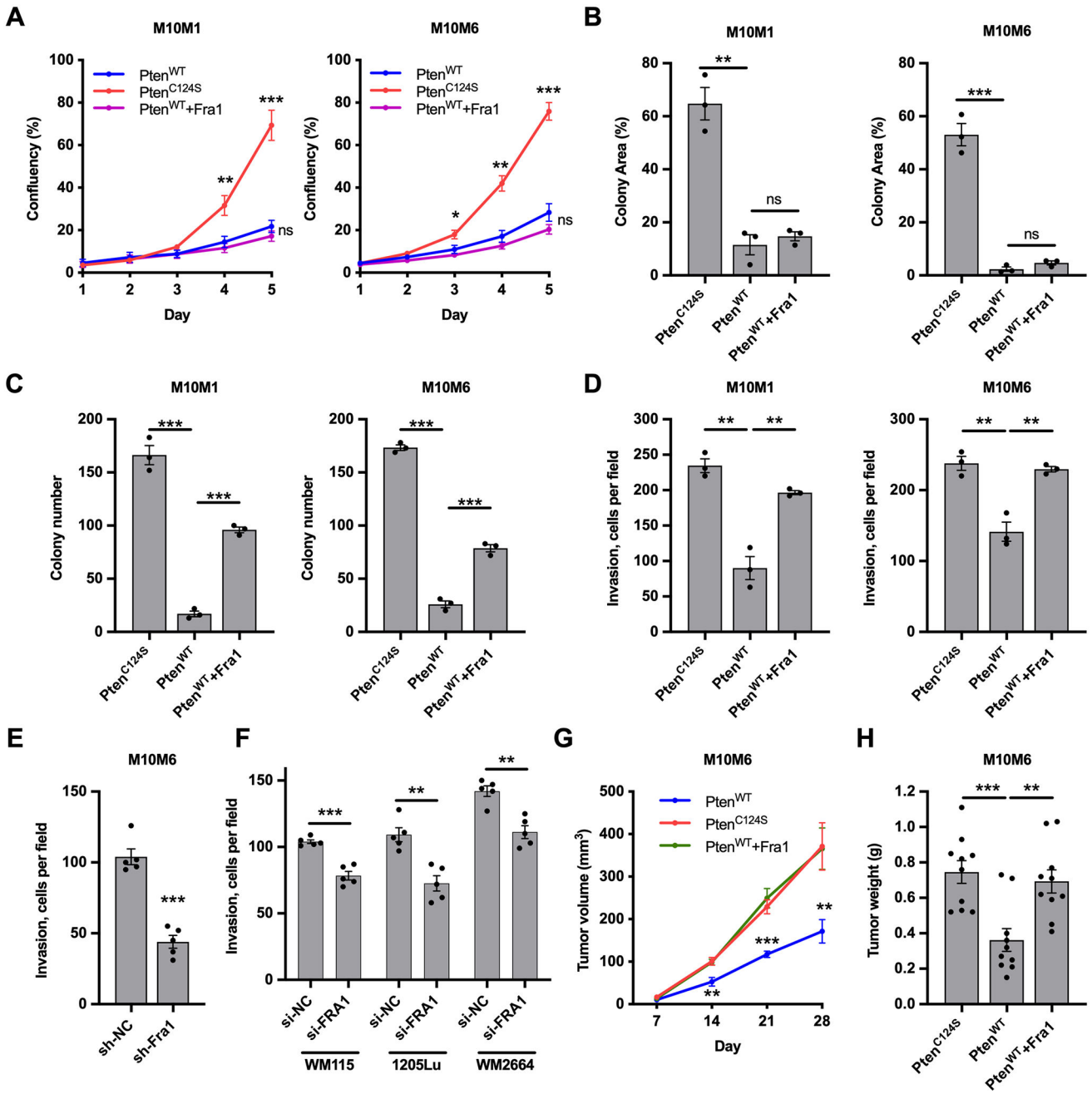

Figure 8. FRA1 overexpression partially abrogates melanoma suppression by PTEN.

A, Proliferation as measured by relative confluence of M10M6 and M10M1 cells expressing Pten^{WT} or Pten^{C124S} or Pten^{WT}+Fra1. **B,** Quantification of percentage occupied area of low-density colony formation assays of M10M6 and M10M1 cells expressing Pten^{WT} or Pten^{C124S} or Pten^{WT}+Fra1. **C,** Quantification of colony number of anchorage-independent growth of M10M6 and M10M1 cells expressing Pten^{WT} or Pten^{C124S} or Pten^{WT}+Fra1. **D,** Quantification of cell numbers of transwell invasion assays of M10M6 and M10M1 cells expressing Pten^{WT} or Pten^{C124S} or Pten^{WT}+Fra1. **E-F,** Quantification of cell numbers of transwell invasion assays of FRA1 silenced mouse melanoma cells M10M6 (E) and human

melanoma cells WM115, 1205Lu, and WM2664 (F). **G-H,** M10M6 cells expressing $Pten^{WT}$ or $Pten^{C124S}$ or $Pten^{WT}$+Fra1 were subcutaneously injected into NSG mice (n=10). Mice were fed chow containing 200 mg/kg Doxycycline to induce expression of PTEN mutants. Tumor volumes were measured every 3 days. The curves of tumor volume (G) and the tumor weight at the end point (H) are shown. Mean ± SEM are shown in (A-H). Data are analyzed with Student's unpaired *t* test, * P<0.05, ** P<0.01, *** P<0.001.